Author:
Yusuf, Ibrahim

Title:
Crustal structure of the Horn of Africa and southern Gulf of Aden
evidence from receiver functions on Somaliland

School of Earth Sciences

Crustal structure of the Horn of Africa and southern Gulf of Aden: Evidence from receiver functions on Somaliland

Ibrahim Yusuf

A dissertation submitted to the University of Bristol in accordance with the requirements for award of the degree of Masters by Research in the school of Earth Sciences, in the Faculty of Science.

July 2022

Supervisor: James Wookey

Word count: 15,326

Abstract

Rifts play a vital role in shaping our planet as they result in the breakup of continents and the subsequent formation of ocean basins. This thesis uses applied receiver function analysis and stratigraphic analysis to investigate the crustal structure of Somaliland (northern Somalia), and to assess its crustal deformation history. Previous studies of crustal deformation in Somaliland have used stratigraphic analysis (so-called 'backstripping'). These show evidence of distinct three phases of rifting: 145 Ma-157 Ma; 84 Ma- 66Ma and 23 Ma- 33Ma. We repeat this analysis with an updated porosity model and verify these results. However, this type of study cannot not directly image crustal structure. For this purpose, five broadband seismic stations were deployed in a 260 km long, North-South array from the Gulf of Aden coast to the Somaliland interior. From 9 months of data from the array we identify about 13 earthquakes of sufficient size and at appropriate epicentral distance from further analysis. We apply extended time multi-taper frequency domain cross-correlation receiver function (ETMRF) estimation to the data for these events and use the H-κ stacking method to constrain crustal thickness and v_P/v_S ratio beneath the stations. Three of the five stations (HAG, BUR and DHE) provide a robust result, and we are able to retrieve a partial result for a fourth (EDH). We find that the Somaliland region is characterized by a general trend of increasing crustal thickness from the north to south from ~23 km at the coast with the crustal thickness at its highest (38±4 km) in the mountainous regions, which we infer to be due to the intense rifting processes the region has undergone. This structure also mirrors that of Yemen (on the other side of the Gulf of Aden), suggesting a strong symmetry to the rifting the region has undergone.

Acknowledgments

First and foremost, I would like to thank everyone who has helped me throughout my Masters project. I would like to thank my supervisor James Wookey who has been patient and incredibly helpful with his reassurance and his instant feedback. I would like to thank Professor Mohammed Ali who helped provide the seismometers used in this project and for his scientific insight. I would also like to thank the data collection crew without you I would not have been able to do this project.

Finally, I would like to dedicate this project to my family who have been an immense emotional support throughout my Research project.

Author’s declaration

I declare that the work in this dissertation was carried out in accordance with the requirements of the University's Regulations and Code of Practice for Research Degree Programmes and that it has not been submitted for any other academic award. Except where indicated by specific reference in the text, the work is the candidate's own work. Work done in collaboration with, or with the assistance of, others, is indicated as such. Any views expressed in the dissertation are those of the author.

SIGNED: .....Ibrahim Yusuf..... DATE: ....04/07/2022.....

Students must sign the examination copies but should only print their name in the final version that they electronically submit so that no personal signifiers are shown in the online release of the dissertation.

TABLE OF CONTENTS

List of Figures

List of Tables

CHAPTER 1: Introduction

1.1 Motivation

The complex tectonic structure of the Horn of Africa (northern Somalia)-Yemen conjugate margin has puzzled researchers for many years. This margin formed after the opening of the Gulf of Aden and the rifting of the African and Arabian plates during the Oligocene-Miocene period (Ali and Watts, 2013). The Gulf of Aden is considered a young oceanic rift, and many of its margins have been previously studied, but the crustal structure of Somaliland and how its history of rifting has affected it is much less well known (Ali and Watts, 2013).

This project seeks to investigate the physical and structural factors that have affected the crust beneath the Somaliland region, using seismic methods (particularly receiver functions) to support stratigraphic analysis (backstripping) of well data. The combination of this will provide new constraints on the history of rifting, and the degree of crustal deformation experienced by the region.

1.2. Rifting

Rifted continental margins form after the formation of new ocean basins and the breakup of continents. Continental breakup is the interactions between plume-lithosphere (Cloetingh et al., 2013), when a high temperature, low density mantle plume is separated from large scale convection motions it rises up to the base of the lithosphere from the core-mantle boundary (Cloetingh et al., 2013, Sleep, 2006). Well known rifted margins include the eastern Somalia margin (formed during the Middle Jurassic era where the Madagascar-Seychelles-India block was separated from Africa (Bossuyt and Milinkovitch, 2001)) and the South Namibia margin which was formed following the break-up of Gondwana 180 Ma (Sapin, Ringenbach and Clerc, 2021). The initiation and evolution of rifts play a significant role in the processes of plate tectonics such as the formation of Earth's crust where rifting leads to seafloor spreading in result forms new ocean crust. The timing, cause and style of rift initiation can tell us a great deal about the tectonics of that region (Su et al., 2021) such as its geological history and its magmatism. Rifting processes also have a large effect on the surrounding crustal structure. There are two main models which describe the evolution of such rifts, and their ultimate

expression in crustal structure, the so-called ‘McKenzie’ and ‘Wernicke’ models. These two models predict very different resulting crustal structure, in particular in the symmetry (or lack thereof) around the rift axis.

1.2.1 ‘McKenzie’ model

The first of these is the ‘McKenzie’ model (McKenzie, 1978) (Figure 1.1). This model proposes that, for a given vertical column of crust the lithosphere will be equally stretched thus allowing an instantaneous initial stretch associated with subsidence. As the crust thins, and the rifting progresses, the heat flux increases, and thus the temperature of the shallow rocks rise. This is an effectively pure shear mechanism; this model assumes the stretching is symmetrical.

After a period of rifting has stopped, the crust starts to shrink, cool, and collapses. The sedimentation continues, but now infills a subsiding basin. Another episode of subsidence, known as thermal subsidence, is caused by an increase in density pulling down the lithosphere from below. Because it is attempting to preserve isostatic equilibrium while the upwelled asthenosphere cools, the second subsidence develops exponentially and considerably more slowly than the rapid initial subsidence.

1.2.2 ‘Wernicke’ model

The second model is the ‘Wernicke’ (Wernick, 1985) model based upon a simple shear regime (Figure 1.1). This suggests that a large-scale detachment fault extending through the upper crust to the lower lithosphere and potentially even the asthenosphere accommodates extension in the basin. This predicts a strongly asymmetrical crustal structure.

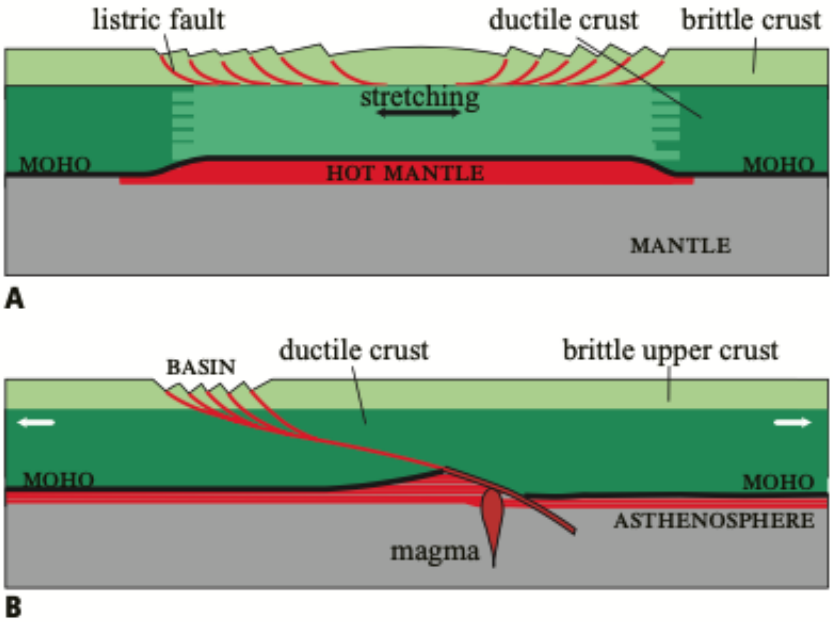

Figure 1.1. Comparative models of rifting. A-pure shear (McKenzie, 1978). B-simple shear (Wernick, 1985). From Doglioni (2008).

Recent studies in areas near the Red Sea rift show that the Wernicke model (simple shear) is favored more in regions near Somaliland (e.g., Cochran et al., 1993) the data in this study correlated to the thermal models of simple shear and fit the heat flow as well as the subsidence data in the rift (Roger, 2004), however there are some problems associated with this model as it does not take into account the effects of melting during the rifting process (Bastow et al., 2005). Kendall et al (2016) also explains that the two stretching models tend to neglect the effect of magmatism as well as heating during the rifting process, this could potentially be difficult as melting plays a significant part in lithospheric stretching and it facilitates the rifting process, the melt can also reduce the strength of a plate by focusing the strain when there is little crustal stretching (Buck, 2004; Roger, 2004; Kendall et al, 2016). By studying other, less-well known rifted margins we can form a better understanding of rifting on continental margins – the Horn of Africa presents such an opportunity.

A complicated and active geological history of rifting and breakup may be found in the Red Sea and Gulf of Aden. The Red Sea started to form as a result of the divergent plate boundary between the Nubian and Arabian plates during the Late Miocene epoch, according to recent findings by Bellahsen et al. (2021) (11-5 Ma). During the Early Miocene, the Afro-Arabian plate rifted and split into the African and Arabian plates, resulting in the formation of the Gulf of Aden (23-15 Ma). Leroy et al. (2019) also found evidence of multiple phases of

rifting and volcanism along the Red Sea and Gulf of Aden margins, leading to the development of large rift basins and transform faults. Furthermore, Bosworth et al. (2020) demonstrated that the ongoing tectonic activity along the Red Sea and Gulf of Aden is likely to play a major role in shaping the future evolution of these regions.

The complex tectonic history of the Red Sea and Gulf of Aden has been the subject of extensive research over the past few decades. In addition to the findings by Leroy et al. (2019), and Bosworth et al. (2020) mentioned earlier, other studies have shed light on various aspects of the rifting and breakup process. For example, Kusznir et al. (2018) used 2D and 3D numerical models to investigate the role of lithospheric thickness, extension rate, and mantle temperature in controlling the development of the Red Sea and Gulf of Aden rift systems. Their results suggest that lithospheric thinning and associated magmatism are the key factors that drive the rifting and breakup process. Similarly, Hamoudi et al. (2019) analyzed the magnetic anomalies along the western margin of the Gulf of Aden and found evidence of multiple phases of seafloor spreading and transform faulting. Their data support the idea that the Gulf of Aden underwent a complex evolution involving repeated phases of rifting, subsidence, and oceanic crust formation. Overall, these studies highlight the complex and dynamic nature of the Red Sea and Gulf of Aden rift systems and provide important insights into the processes that shape the Earth's crust.

1.3 Tectonics and Crustal Structure of the Horn of Africa.

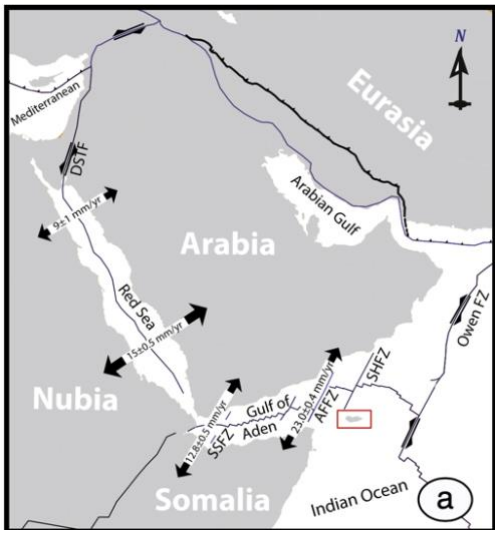

Figure 1.2. Tectonic context of the Somaliland region. The red box denotes the island of Socotra (from Ahmed et al., 2014). The acronyms (e.g., AFFZ: Alula Fartak fracture zone

In the Horn of Africa, three major plate boundaries intersect. These are the Red Sea and Gulf of Aden oceanic spreading ridges, and the continental East African Rift system. The effect of these tectonic systems dominates Somiland's shallow crustal structure (Figure 1.2) (Fairhead and Girdler, 1972). The Gulf of Aden has undergone extensive extensional tectonics during its opening which has preceded a system of east to west normal faulting trends (Ali, 2009) towards the north. The Red Sea faulting trend is also seen although not commonly in a series of NW-SE striking faults (Hunt, 1942). What is less well known, however, is how this is reflected in the deeper structure of the Somaliland's crust.

The crustal structure in the region around Somaliland has been previously studied. Dugta et al. (2005) investigated the crustal structure in Kenya and Ethiopia (to the south of Somaliland) using receiver function analysis. They discovered that to the east of the Kenyan rift the crustal thickness fluctuates between 39 and 42 km (Dugda, 2005). The crustal thickness in the Afar Depression was discovered to be 25 km as well as the crustal thickness ranging from 33-34 km beneath the Ethiopian Plateau on both sides of the Ethiopian Rift (Dugda, 2005).

Ahmed et al. (2013) analysed P-wave receiver functions in western Yemen, on the other side of the Gulf of Aden rift. They show that on the Yemen plateau, the crust is a ~35 km thick. This thins to less than 14 km along the Red Sea coast and to ~22 km in coastal areas (Dugda, 2005). In addition, Ahmed et al. (2014) investigated crustal structure of Socotra Island using receiver functions. They show that in central Socotra it has an average crustal thickness of ~28km and it decreases westward along the margin to an average of ~21km (Dugda, 2005).

However, there have been no studies conducted to image the deep crustal structure of the rifted margins and plateau of the Horn of Africa (northern Somalia) and to critically evaluate crustal scale deformation history and evolution during rifting. Quantifying the degree of tectonic stretching and magmatic addition during continental rifting depends heavily on variations in crustal thickness and the assessment of magmatic input. Therefore, the primary aim of this project is to constrain and examine the nature of the rifted continental crust and plateau of the northern Somalia by constraining Moho depths.

1.4 Geology of Somaliland

1.4.1 Gemorphology

The broad morphology of Somaliland is similar to areas that have undergone extension such as Yemen, with basins and mountains of elevations up to 2000 m. There is little folding, but extensive normal faulting (roughly NW-SE), some of which has very significant throws (Ali, 2015). Since the Lower Jurassic, these strong vertical movements have restricted the accommodation space for sediment deposition (Ali, 2015).

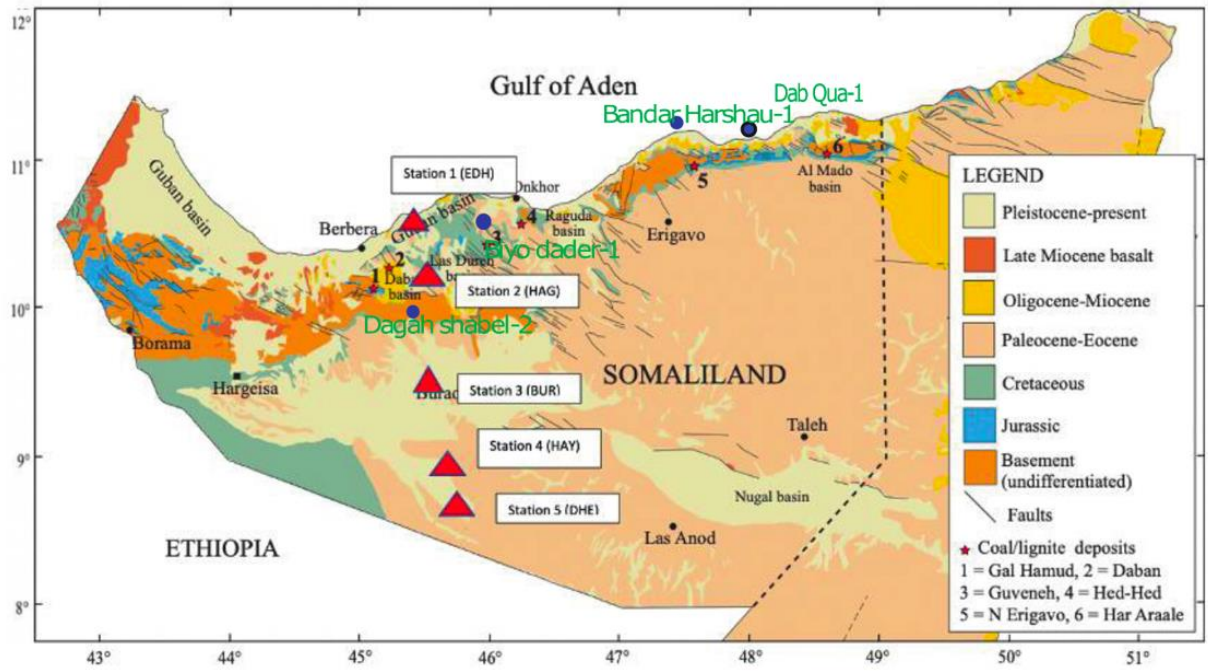

Figure 1.3. Simplified geological map of Somaliland (modified from Ali, 2009). The red triangles show the locations of the 5 seismometers used in Chapter 3 and 4, as well as the 4 wells used in Chapter 2 and the blue circles indicate the well locations.

1.4.2 Stratigraphic and Depositional Setting

The sedimentary section in Somaliland can be divided into three parts: Jurassic rift sequences, cretaceous sequences and the Tertiary sequence (Eocene sequences and Oligocene-Miocene sequences) (Ali, 2009).

The Jurassic rift sequence (200 Ma-145 Ma): The Jurassic deposits of Somaliland consist of continental deposits and are overlain by a sequence of limestones. The Jurassic sediments

were deposited in NW–SE trending grabens that were created by tensional forces linked with the rifting of India and Africa (Bosellini, 1992; Ali, 2009).

The Cretaceous rift sequence (145 Ma-66 Ma): The cretaceous rocks of Somaliland lie unconformably over the Jurassic rocks this is due to major faulting and crustal uplift before the Cretaceous sedimentation (Bosellini, 1986; Ali, 2009). This sequence consists of sandstone characterized as Nubian sandstone (Macfadyen, 1933) as well as Yesomma Sandstone in which crustal uplift can be seen in western Somaliland.

The Tertiary rift sequence consists of the Eocene sequence (55 Ma-34 Ma) and the Oligocene-Miocene sequences (34 Ma-5 Ma). Tertiary rocks occupy most of the surface exposures in Somaliland and lie conformably over the Cretaceous sequence. The main deposits of the Eocene sequence are gypsum rich limestones The Oligocene-Miocene sequence deposits are mostly seen along the costal belt of the Gulf of Aden, they consist of red, green sand, siltstone and gypsiferous sandstone (Bosellini, 1992; Ali, 2009).

1.5 Aims and Objectives

The aim of this study is to image the deep crustal structure of the rifted margin in Somaliland and evaluate the crustal scale deformation history using seismology (specifically receiver functions). We will use data from a new temporary deployment of five broadband seismometers across central Somaliland, as well as a stratigraphic analysis of well log data.

The larger goal of this thesis is to contribute to the body of knowledge regarding the crustal structure using comparisons to receiver function studies of Yemen (on the other side of the Gulf of Aden rift). This project aims to compare the trend of the variation of crustal thickness in Yemen with that of Somaliland and the implications for past rifting in the Somaliland region.

Finally, this project aims to determine the extent to which the three rifting events during the late Paleogene and early to mid-Mesozoic rifting have modified the thickness and composition of the crust in which the Somaliland-Yemen conjugate margin formed by comparing well data with receiver function data.

CHAPTER 2: Analysis of Somaliland's Rifting History from Backstripping Analysis

[Data and tools for the backstripping analysis presented in this chapter were provided by Prof. Mohammed Ali (Khalifa University), who also assisted with the interpretation of the results.]

Stratigraphic information can be used understand the rifting history of Somaliland, and to determine the extent of its impact on Somaliland's crustal structure. In this chapter we review previous work using stratigraphic 'backstripping' to quantify this rifting history, and we repeat the calculations of Ali and Watts (2013, 2015) with updated porosity values, and outline the resulting intepretation of the crustal structure.

2.1 Methodology

The backstripping technique was first used by Watts and Ryan (1976) in a study of the subsidence of the Atlantic margins. Since then, it has become a widely practiced geophysical technique (e.g., Roberts et al., 1998; Fang et al., 2022).

Backstripping is a method used to analyse a basin's subsidence history by simulating a gradual reversal of the depositional process (Roberts et al., 1998). The application of the backstripping technique involves two main steps. The first is 'decompaction'. This aims to restore the original thickness of sediment layers in the stratigraphic column prior to compaction by loading of subsequent units. The recovered sediment thickness is then used to gradually unload basement lithological units while accounting for isostasy, along with a model of changes in water depth and long-term sea level (Ali and Watts 2013). Backstripping results in the division of the sediment buildup into two components: the first is the sediment contribution and water loading, and the second is the unidentified tectonic subsidence and uplift (Steckler et al., 1999; Ali and Watts 2013; Allen and Allen, 2013).

2.1.1 Calculating decompaction

As they are deposited and eventually buried, sediments are compacted by the weight of the sediments above them (Holt, 2012). In order to backstrip multiple layers all the stratigraphic units in a sequence needs to be restored for each timestep by decompacting the younger units and compacting the older units. Figure 2.1 shows the process of a current sedimentary column being decompacted through time. The deepest layer (1) is decompacted in column (1) to give us the second column at time 1. Subsequently layers are added as time passes. In time 2 the deepest layer is compacted a little bit, but the new layer above remains uncompacted. As time passes the layers even out to match the current thicknesses. This shows that to backstrip multiple layers all the stratigraphic units need to be "restored" in a sequence for each time step, thus decompacting the younger units and compacting the older units (Allen and Allen, 2005).

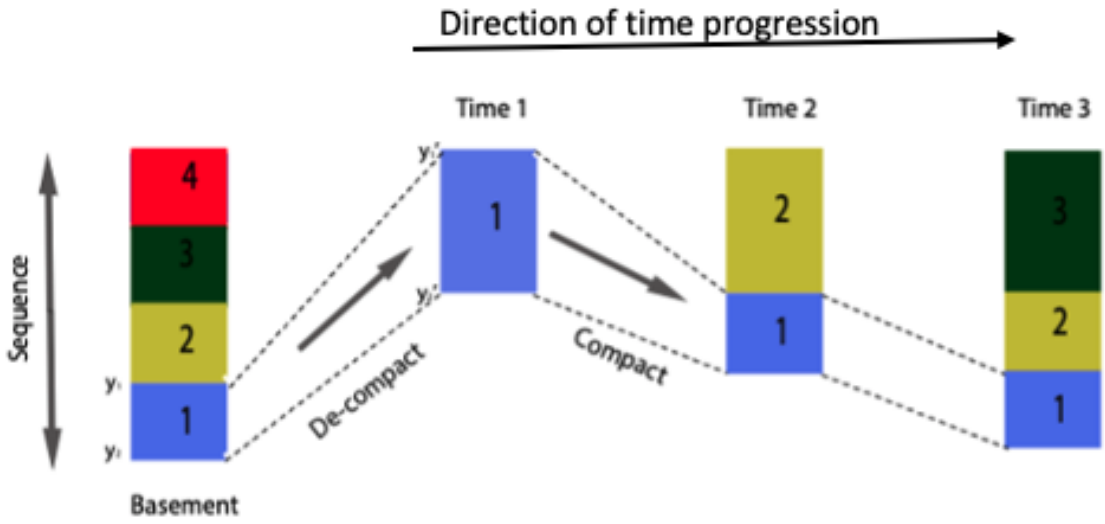

Figure 2.1. Timeline of the decompaction process. Where numbers 1,2,3 and 4 represent layers in a sedimentary column and 1 being the deepest.

Figure 2.1. Timeline of the decompaction process. Where numbers 1,2,3 and 4 represent

Compaction causes a change in dimensions of a volume of sediment due to gravitational loading of overlying water-saturated sediment (Allen and Allen, 2005). This plays a big role when sediments are deposited due to the sizeable amount of pore space between the grains filled with water or another fluid (Jiaren and Mingde, 1997; Holt, 2012).

The pore space will start to reduce as new sediments are added on top of the first sediment layer (e.g., Holt, 2012; van der Land et al., 2013), due to grains becoming deformed, pore

space closing and water being expelled. This is a result of the effective stress (*s*, defined as vertical compressive stress minus fluid pressure) on the sediment (Swarbrick, 2012).

This process is known as mechanical compaction and is dependent on pressure, as well as the composition of the sediment grains, for example, lithic grains deform much easier than silica grains (Holt, 2012; Martín-Martín and Robles-Marín, 2020). Porosity loss in basins may also be a result of chemical compaction which involves the cementation of grains when deposited and the filling of pore space by chemical precipitation. This is highly dependent on temperature rather than loading. Backstripping analysis mainly considers mechanical compaction due to changes in temperatures being hard to constrain (Martín-Martín and Robles-Marín, 2020).

The 'pre-compacted' sediment layer will have a porosity which varies with depth influenced by the lithological character of the strata which must be accounted for. Rock deformation tests and measurements taken in a natural subsurface environment are used to make observations about the porosity-depth relationship of sedimentary rocks. Compaction rate is a significant function of mineralogy, according to tests on rock deformation (Allen and Allen, 2005). Porosity can be assessed on core and sidewall cores retrieved from a borehole, and indirect methods can be used to determine how porosity is distributed with depth in a borehole most commonly through sonic logs this method can only be used if the lithology is known or it can also be determined through neutron and density logs (Allen and Allen, 2005). A common approach where specific lithological information is missing is to assume an exponential decay function (Equation 1). This predicts a decreasing rate of porosity loss representing initial grain realignment and then grains warping (Allen and Allen, 2005). This is the function used in this thesis, and takes the form:

$$\emptyset(y) = \emptyset_0 \exp(-cy). \qquad (2.1)$$

where $\emptyset$ is the porosity at depth, $\emptyset_0$ is the original porosity of the layer when it was deposited, c is the compaction coefficient, and y is the depth. The relationship in (1), and the values commonly used for compaction coefficient and original porosity, are an estimated best fit from a compilation of subsurface data (Allen and Allen, 2005). In studying the subsidence in sedimentary basins, it is typical to presume that the solid volume does not change during burial so that the mechanical compaction of the grains as a result of increasing

compression from the underlying sediment-water column alone is what reduces porosity (Allen and Allen, 2005).

Decompaction, can therefore be estimated from the current layer thicknesses and assumptions about the porosity. This approach – from (Angevine, Heller and Paola, 1990; Steckler and Watts, 1978) – is outlined below:

The total volume of a rock layer for a one-dimensional column is given by its thickness:

$$V_T = y_1 - y_2. \qquad (2.2)$$

where V_T is the total volume of a rock layer, and $y_2 - y_1$ is the thickness of layer 1 in the present day. Using the exponential relationship between porosity and depth (1), the present volume of water-filled pore space in the layer can be found by taking the integral of the exponential across layer 1:

$$V_w = \int_{y_1}^{y_2} \emptyset_0 \exp(-cy)\, dy. \quad (2.3)$$

Thus

$$V_w = \frac{\emptyset_0}{c}(\exp(-cy_1) - \exp(-cy_2)). \qquad (2.4)$$

The volume of water-filled pore space in the layer before compaction (time 1 in figure 5) can also be found by integrating over the bottom of the decompacted layer ($y_2{}'$), and the top of the decompacted layer ($y_1{}'$), where the prime superscript denotes the decompacted layers.

$$V_w' = \frac{\emptyset_0}{c}(\exp(-cy_1{}') - \exp(-cy_2{}')). \qquad (2.5)$$

When a layer is subjected to mechanical compaction the volume of the pore space changes due to sediments expanding when moving to new depths, the volume of the sediment grains is therefore given by the change in thickness of the decompacted layer:

$$V_w' = y' - y_s. \qquad (2.6)$$

Where y' is the layer's thickness before compaction and y_s is the thickness of the sediment grains.

Combining the two equations for the compacted layer:

$$y' = y_s + \frac{\emptyset_0}{c}(\exp(-cy_1') + \exp(-cy_2')). \qquad (2.7)$$

In order to solve for y' we need to solve for y_s', and since the sediment volume does not change during compaction (i.e., $y_s' = y_s$), we can replace y_s in the volume equation,

$$V_w = y - y_s'. \qquad (2.8)$$

where *y* is the present-day thickness $y_2 - y_1$. Substituting this into the present volume of water-filled pore gives and the equation for the thickness of the sediment grains before compaction:

$$y_s' = y_2 - y_1 - \frac{\emptyset_0}{c}(\exp(-cy_1) - \exp(-cy_2)). \qquad (2.9)$$

The decompacted thickness is given by

$$y' = y_2' - y_1'. \qquad (2.10)$$

Substituting the decompacted thickness equation (2.9) and the equation for the thickness of the sediment grains (2.10) before compaction into the equation for the thickness of the layer before compaction (2.7) finally gives us the decompaction equation (e.g., Taylor, Nicol and Walsh, 2008):

$y_2' - y_1' = y_2 - y_1 - \frac{\emptyset_0}{c}(\exp(-cy_1) - \exp(-cy_2)) + \frac{\emptyset_0}{c}(\exp(-cy_1') + \exp(-cy_2'))$.
(2.11)

2.1.2 Correcting for Weight of Sediments

The second set of effects we need to correct for is sediment loading and sea level change. The weight of the sediments can be corrected by for calculating and correcting for the effect of subsidence (Allen and Allen, 2005).

The subsidence calculated assuming a basin filled with water instead of sediments (Holt, 2012). Airy isostacy, which asserts that at compensation depth the weights of the two columns are balanced, is used to calculate tectonic subsidence *Y* (Holt, 2012).

The sediment grain density/ bulk density of a decompacted layer can be calculated using:

$$\begin{aligned} V_t &= V_w + V_{g.} \\ m_t &= m_w + m_{g.} \\ \overline{\rho}_{si} V_t &= \rho_w V_w + \rho_{gi} V_{g.} \\ \overline{\rho}_{si} &= \rho_w \emptyset_{si} + \rho_{gi}(1 - \emptyset_{si}). \end{aligned} \qquad (2.12)$$

where $\overline{\rho}_{si}$ is the density of a decompacted layer, ρ_{gi} is the sediment grain density, m_g is the mass of the grains and V_g is the volume of the grains.

2.1.3 Correction for Sea Level Change

The next stage is to take into consideration the weight effects of the water column once the sediments have been decompacted and the sedimentary load at each time interval has been corrected (Holt, 2012). At every time step, the top of the sediment column must be adjusted to the same datum (in this case the current sea level) in order to trace the subsidence through time (Holt, 2012). Since sea level is the datum from which subsidence is calculated, it is crucial to adjust sea level fluctuations as they may result in inaccuracies in the calculation of the basin's subsidence history. For example, the record will indicate increasing water depth if sea level increases. This can be used to mean that basin subsidence is increasing, and vice versa (Allen and Allen, 2005, Holt, 2012).

Water depth can be extremely hard to interpret. The most popular way to calculate it is to do a biostraticgraphic study, fossil assemblage in sediments along with stratigraphic data is used

to estimate the water depth when deposited (Allen and Allen, 2005; Holt, 2012). For shallower depth (under 200 m) calculating the water depth is more straightforward as the errors will be much less. Once calculated the water depth is subtracted from the subsidence to minimize the effect (Holt, 2012).

The final result of these corrections is to account for the increasing loss of porosity with depth of burial for decompaction corrections, as well as to account for changes in paleosea-level relative to today.

2.2 Previous Studies of Somaliland-Yemen Conjugate Margin Using Backstripping

The effect of crustal structure due to rifting in Somaliland and in particular its comparison with Yemen, has been previously studied using backstripping of biostratigraphical data by Ali and Watts (2013; 2015, hereafter A&W). They use 8 wells located in the Somaliland-Yemen conjugate margin. They apply the technique outlined above (Watts & Steckler, 1979) with porosity information and water depth information calculated using parameters from surrounding lithology.

2.3 Updated Backstripping Analysis

Here, we revisit the backstripping analysis of A&W on a subset of the four wells on the Somaliland side of the rift, with a recalculated porosity model (the original porosity model was unavailable) in order to test and verify their results and interpretations of Somaliland structure and provide context for the later seismological study. In our calculations the porosity was estimated from well log data using the neutron-gamma ray log method for Dab Qua-1 and Banda Harshau-1 (Figure 2.2) following the method of Ali and Watts (2015). No neutron-gamma ray well log data were available for Biyo Dader-1 and Dagah Shabel-2, and a simple model of reducing porosity with depth was used (Figure 2.2).

Figure 1.3 shows the location of the exploration wells with two offshore wells (Bandar Harshau-1 and Dab Qua-1) along the coast of Gulf of Aden and two onshore wells (Biyo Dader-1 and Dagah Shabel-2) near the seismic array described in the next chapter.

To quantify the tectonic subsidence and calculate the uplift curves from backstripping analysis assumptions on the densities of water and mantle were made of 1030 and 3330 kgm^{-3} respectively (Ali and Watts, 2015). An assumption on the Airy isostasy is made, this is key when backstripping as it ensures that the weight of two layers is the same at the compensation depth (Allen and Allen, 2005). Table 2.1 outlines the parameters used, the same parameters as used by Ali and Watts (2015) were used in this study.

Parameter	**Value**
Density of water	$1030\ kgm^{-3}$
Density of sediment grains	$2670\ kgm^{-3}$
Density of crust	$2800\ kgm^{-3}$
Density of mantle	$3330\ kgm^{-3}$
Thickness of zero elevation crust	31.2 km
Young's modulus	100 GPa
Poisson's ratio	0.25
Thermal thickness of the lithosphere	125 km
Temperature at base of lithosphere	$1333\ °c$
Coefficient of volume expansion	3.28×10^{-5} ℃

Table 2.1. Parameters Used in the Thermal and Mechanical Modelling from Ali and Watts (2015).

2.4 Results

The resulting estimates of tectonic subsidence through time for the four wells are shown in Figure 2.2. All wells show evidence of significant vertical movement through time especially early in the rifting history.

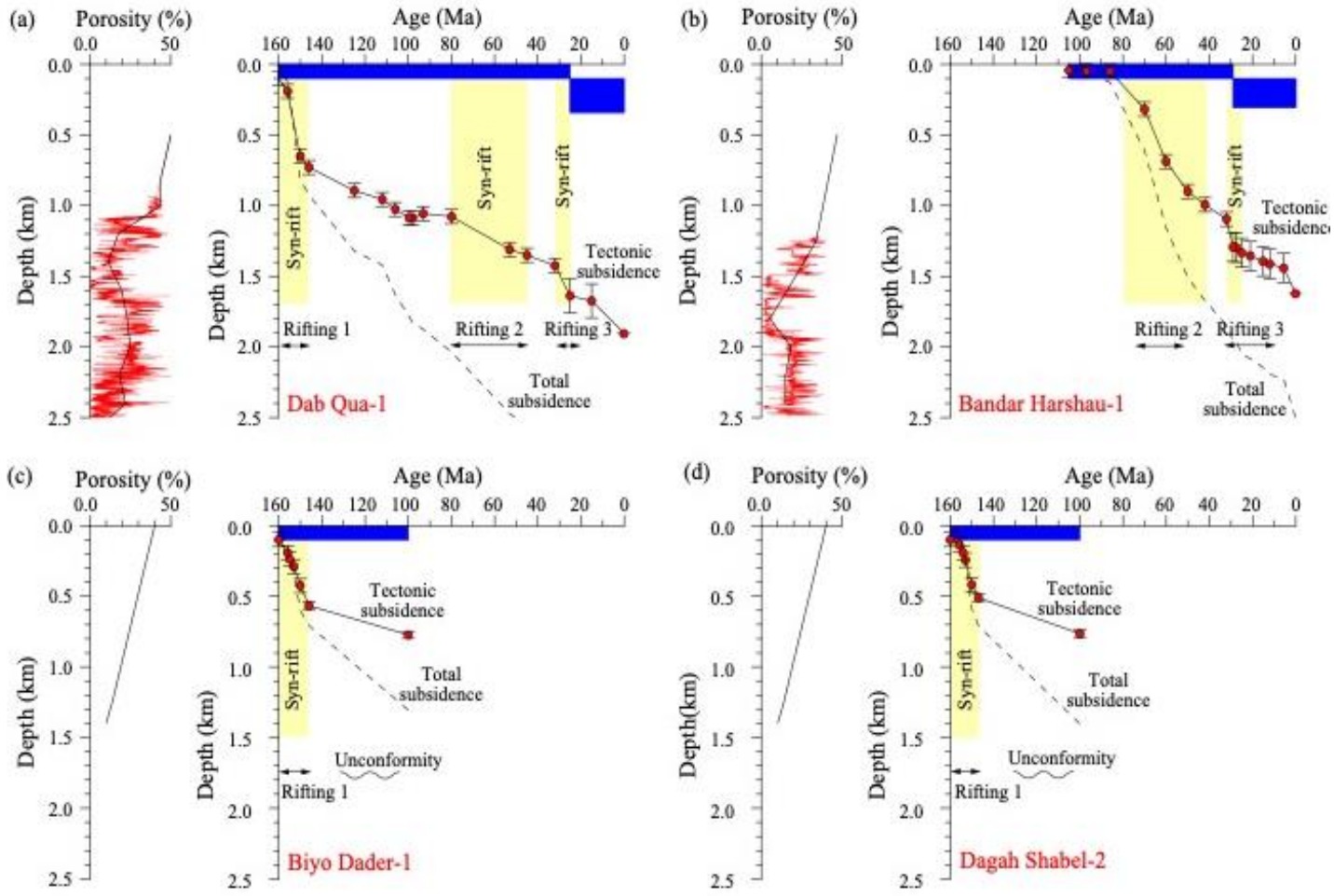

Figure 2.2. Backstripping figures of biostratigraphic data from the 4 wells showing the total sediment accumulation at the well together with the tectonic subsidence. The yellow boxes indicate the rifting periods, and the blue boxes denote the water depth (estimated from Ali and Watts (2015)). No porosity vs depth values were available for wells C and D, so a simple reduction with depth is assumed.

2.5 Interpretation

Our updated subsidence curves show nearly identical results to Ali and Watts (2015). This shows that the updated porosity has little effect on the ultimate results. This could be because there is not a large disparity between the recalculated porosity and the original porosity values, this lends confidence in the interpretation of the curves. The porosity values observed for Dab Qua-1 and Bandar Harshau-1 help us confirm the rift phases seen in the 2 wells as it highlights the changes in porosity at specific stratigraphic intervals.

2.5.1 Rifting Events

The main features in the subsidence curves at the wells in Guban basin are similar. This gives us confidence that we have properly accounted for all the effects in the stratigraphic record at each well and that backstripping does, in fact, separate the key elements of the regional trends of tectonic subsidence and uplift. The tectonic subsidence and uplift curves show four main tectonic features, which we (following A&W) associate with rifting events over the past 160 Myr, starting with the earliest imaged.

Kimmeridgian-Tithonian rift phase (145 Ma-157 Ma):

The first rift phase is the most prominent feature of the backstrip curves seen on all the wells except Bandar Harshau-1, this accelerating subsidence from ~157 Ma to ~148 Ma is interpreted by Ali and Watts (2015) to be a fast initial subsidence which is followed by post rift subsidence due to its concave-up profile. This first rifting period is thought with the breakup of Gondwana (Mason, 1957; Ellis et al., 1996; Ali and Watts, 2015).

Uplift in early to late cretaceous (100 Ma- 145 Ma):

There is second period of tectonic activity shown in the subsidence curves in wells Biyo Dader-1, Dagah Shabel-2, and Dab Qua-1. These subsidence curves are much shallower suggesting a decrease in subsidence this could be due to post rift thermal subsidence. The subsidence curves display unconformities at Biyo Dader-1 and Dagah Shabel-2, Ali and Watts (2015) suggest that it could be linked with the Neocomian-Barremian uplift of the region (Miller, 2005).

Campanian-Maastrichtian rift phase (84 Ma- 66Ma):

This is the second rift phase seen on both offshore tectonic subsidence curves (Dab-Qua-1 and Bandar Harshau-1) it is characterized by a period (~80 Ma to ~48 Ma) of rapid subsidence. It is attributed to the movement of the Indian plate northwards as well as the slowing down of the African plate (Cande and Stegman, 2011).

The tectonic subsidence curves indicate the subsidence rate of the second phase of rifting is faster than the first phase for the Bandar Harshau-1 well. Therefore, the basin infill in Bandar Harshau-1 well is mainly of Campanian age (Ali and Watts, 2015). The differences seen in tectonic subsidence between the two wells could be due to more mantle stretching near the Bandar Harshau-1 well.

Third rift phase: Oligocene-Miocene (23 Ma- 33Ma):

The final rift event spans from 32 Ma- ~28 Ma (rift duration ~4 Ma) and is only seen on the two offshore wells (Dab-Qua-1 and Bandar Harshau-1) (Figure 2.2). In the both wells a rapid rate of subsidence is evident, where Bandar harshau-1 shows a faster rate of subsidence than Dab-Qua-1. This increase in subsidence is thought to be due to the separation of Arabia from Africa and opening of the Gulf of Aden (Ali and Watts, 2013; Ali and Watts, 2015).

2.5.2 Extension Factor

A&W also compare the tectonic subsidence that resulted from backstripping to thermal model predictions (McKenzie, 1978) to confirm the interpretations of Somaliland's rifting history. We also repeat this analysis – Figure 2.3 compares tectonic subsidence with extension factor (crustal stretching). We used a modified form of the McKenzie model, which is based on blocks of finite width and considers the impacts of heat flow, flexure, and rifting during brief periods of time. (Ali and Watts, 2013; Cochran, 1981). In this model, assumptions were made regarding the initial, pre-rift crustal thickness, Tc, which was set at 35 km based on seismic refraction data and receiver function analysis in Yemen (Ali and Watts, 2015, Tiberi et al., 2007; Watremez et al., 2011; Ahmed et al., 2013) the rest of the model parameters used are summarized in Table 2.1. The beta curves further indicates that the region has undergone significant stretching with the beta curves for the first rifting event

yielding a beta stretching factor ranging from 1.00 -1.22 across all 4 wells, for the second rifting event the beta stretching factor ranges from 1.00 -1.25 and for the third rifting event's the beta stretching factor ranges from 1.00 -1.25, the wide range of values observed indicates the region has undergone some form of crustal thinning (Ali and Watts, 2015).

The beta factors were determined through a systematic analysis, involving the division of the subsidence rate by the rate of global sea level change. Subsequently, the beta factors were refined using a rigorous least squares fitting process, ensuring accuracy and reliability in the results.

$$Beta\ factors = \frac{subcidence\ rate}{\text{eustatic sea-level change rate}} \qquad (2.13)$$

Where the subsidence rate is the rate of change of thickness of a sedimentary layer and the reference subsidence rate is a selected value that is used to standardise subsidence rates and facilitate comparisons among various levels (Ali and Watts, 2015).

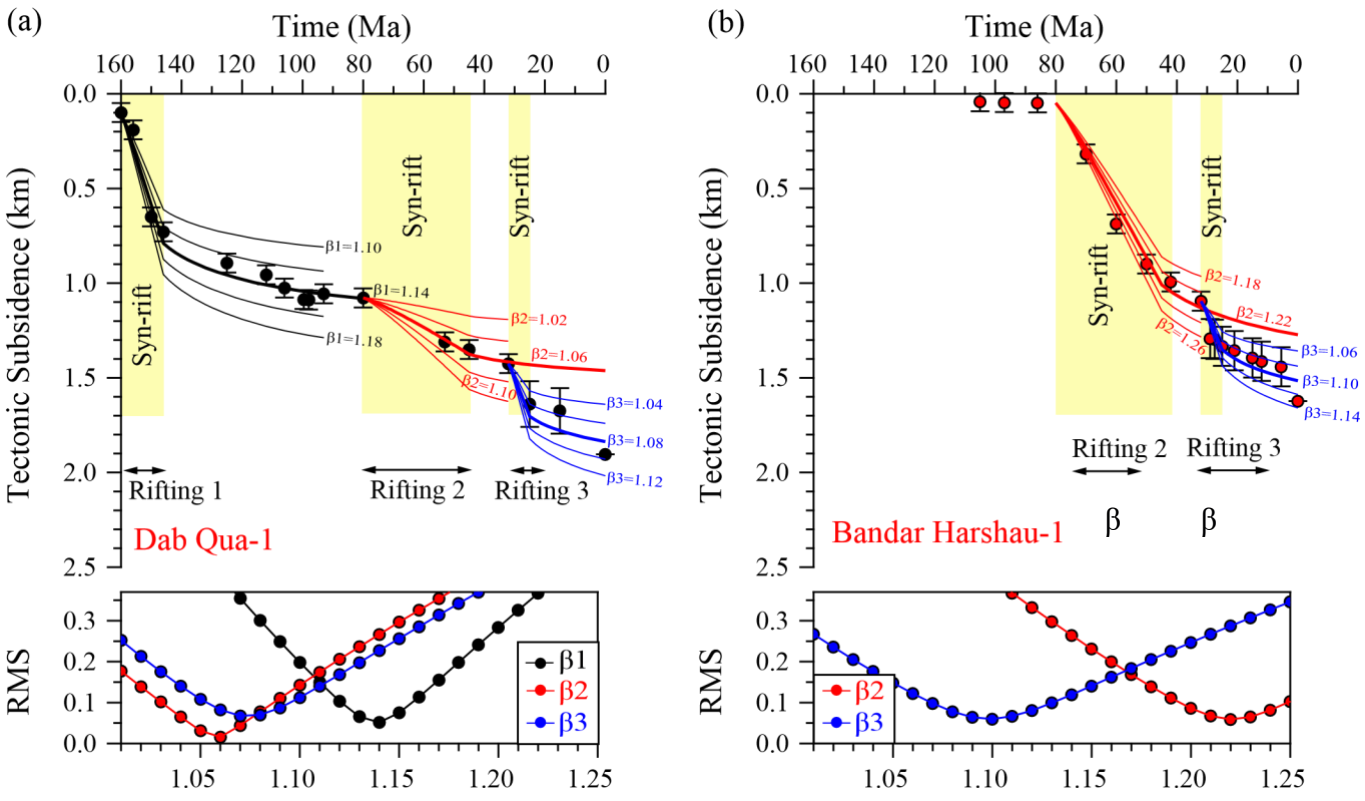

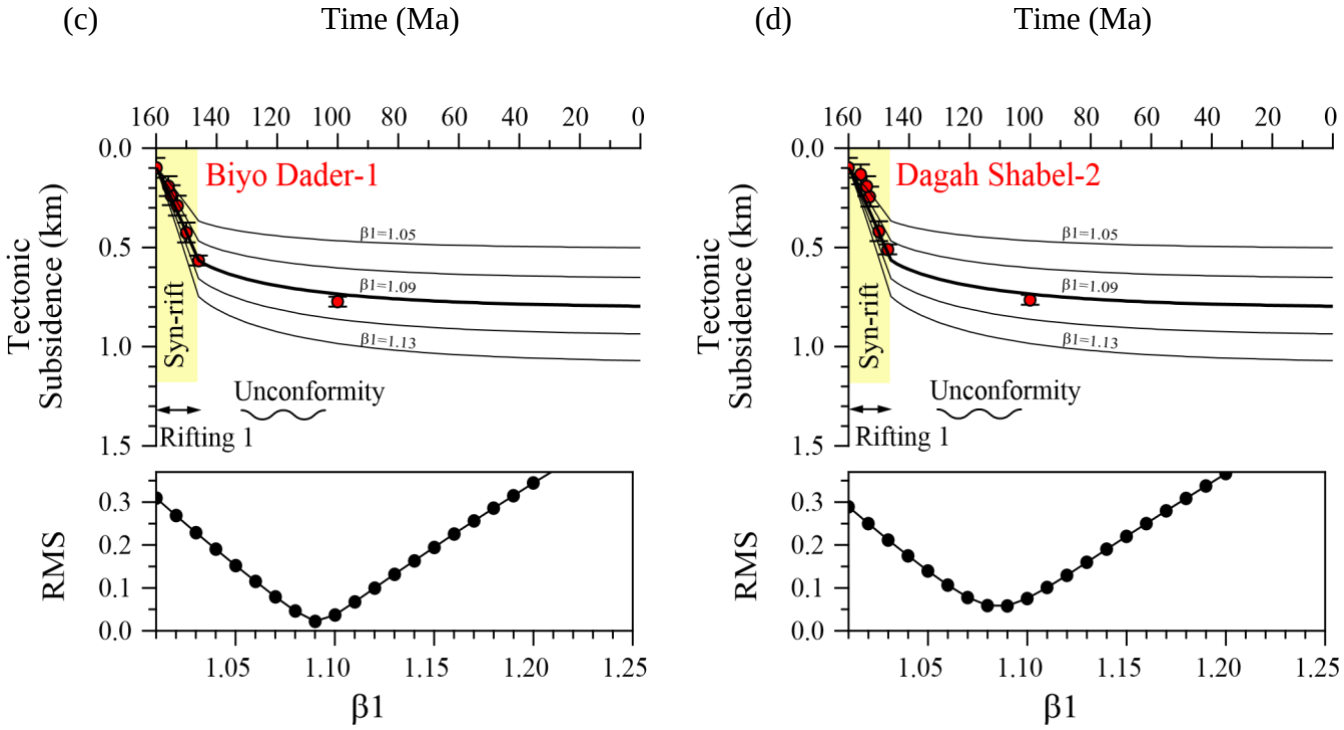

Figure 2.3. Comparison of the backstripping inferred subsidence at 4 exploration wells in the Somaliland region to the predictions of a uniform extension model with crust and mantle extension, β. The figure shows RMS vs beta factors where the RMS value represents the root-mean-square error between the predicted and observed values of relative sea level change over a certain time period, from this we evaluate the accuracy of the subsidence models to assess the impact of uncertainties in the beta factor on the model's accuracy.

2.5.3 Discussion

The results obtained from backstripping the data from the 4 wells broadly reproduce the earlier work by Ali and Watts (2013). Figures 7 and 8 show the backstripped subsidence curves for the 4 wells in northern Somalia. These are very similar to those in shown Ali and Watts (2013), showing the updated discretisation of the porosity data has not changed the results significantly. As discussed in Ali and Watts (2013), the subsidence curves suggest three rifting events that span from the Oligocene- Upper Jurassic Epoch, summarised below.

The first rift phase is the most prominent feature of the backstrip curves and is seen on all the wells except Bandar Harshau-1 and spans from ~157 Ma to ~148 Ma (rift duration ~11 Ma) it is characterized by a steep curve which suggests accelerated subsidence. This has been suggested to be associated with the break-up of Gondwana (Ali and Watts, 2015).

The backstrip curves of the Bandar Harshau-1 and Dab Qua-1 wells suggest a second rift period from ~80 Ma to ~48 Ma (rift duration ~32 Ma). It has been suggested that this phase of rifting is associated with the slowing down of Africa's plate motion and the northward motion of the Indian plate Ali and Watts (2013).

The final rifting event observed from the backstrip curves is observed during the Oligocene-Miocene Epoch from ~32 Ma- ~28 Ma (rift duration ~4 Ma). This is observed on the two offshore wells Bandar Harshau-1 and Dab Qua-1. This rifting period is characterized by rapid subsidence which is attributed to be due to the opening of the Gulf of Aden and the separation of Arabia from Africa (Ali and Watts, 2015).

Analysing the rifting history of Somaliland gives us a better understanding on the crustal deformation history, however, there have been no seismic surveys evaluating the thickness of Somaliland's crust. In the next two chapters we analyse seismic data collected from five seismometers across Somaliland to get a more complete analysis of the crustal structure and deformation history of Somaliland.

CHAPTER 3: Somaliland Temporary Seismic Deployment

[The original project plan was for the author to assist with the deployment and data collection fieldwork associated with this array, in partnership with local collaborators. The travel restrictions imposed during the COVID-19 pandemic unfortunately made this impossible and the fieldwork was done by our collaborators in the region. Data was delivered electronically, and all processing and archiving was done by the author.]

3.1 Seismic Array

This thesis uses data from a small, temporary seismic array in Somaliland (Figure 1.3), acquired for the project. The seismic stations are deployed in an approximately north-south 260km line across Somaliland, from Eiil Deraad to Dheryelle. The stations were deployed in October 2020 to July 2021 totalling approximately 9 months of data. In this thesis, we use data collected in batches from the array collected in January 2021 and July 2021. The locations of the seismometers are summarised in Table 3.1.

The stations in the study comprise broadband Nanometrics Trilium 120 Posthole seismometers, which were installed on concrete base plates and buried in holes 0.5-1 m deep (Figure 3.1). These are broadband, three-component instruments designed for down-hole deployments. They have a flat velocity response between 120 s and 150 Hz and low self-noise (Haberland and Ritter, 2016). They have a flat velocity response between 120 s and 150 Hz and low self-noise (Ringler and Hutt, 2010). The associated digitiser, GPS receiver and solar panels were installed at the surface. The data were recorded continuously at 100 Hz, with waveforms saved to an SD card in the digitiser for retrieval by hand.

The data collections in January and July 2021 resulted in a total of ~1 GB of data in MiniSEED format. The codes to be used in the project rely on SAC (the Seismic Analysis Code), so it was decided to create an archive of the data in SAC format. The conversion was done with a modified version of IRIS code miniseed2sac and the data was saved as a set of 1-day long SAC files.

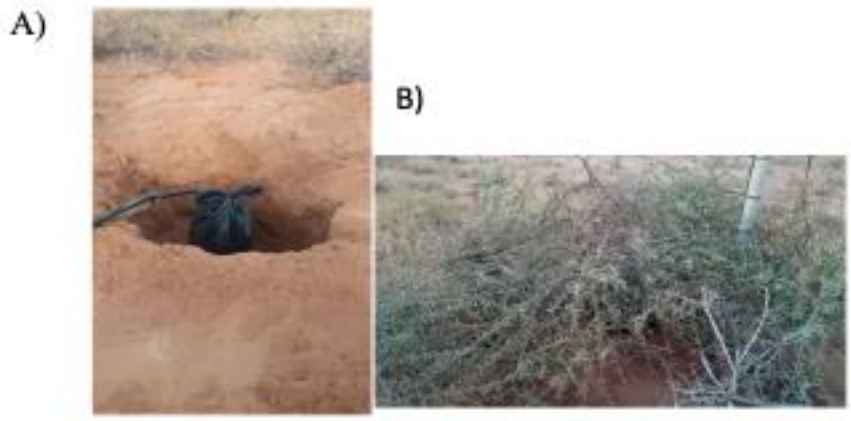

Figure 3.1. Photos showing the installation of the Seismometer in the BUR station where panel A shows the digging for the installation of the seismometer and panel B shows the backfilling and the covering of the hole.

Station Number	Location	Comments
S1H (Site code EDF)	Eil Daraad House N10.72616° E45.57849°	Deployed 17th October 2020 and recovered 8th December 2021, due to traffic noise. The station is located within the fence of the house, this station experienced noise and sensor recalibration issues.
S1 (Site code EDH)	Eil Daraad Farm N10.75869° E45.60419°	Deployed 8th December 2021, same seismometer from the EDF site. Located at the farm. Some days tractors nearby were used to drill holes.
S2 (Site code HAG)	Hagal N10.25256° E45.74044°	Located next to a medical clinic.
S3 (Site code BUR)	Burao N09.51717° E45.56362°	Located in a farm outskirt of Burao.
S4 (Site code HAY)	Haydh Ducato N8.71734° E.45.73534°	Error with the sensor from 19th October 2020-1st January 2021. Re-balanced. All lights are green. The station is next to a house.

S5 (Site code DHE)	Dharyeley N8.39776° E45.83372°	This station is located at a school.

Table 3.1. Table summarising seismometer locations and site information.

3.2 Seismic Noise Characterisation of The Stations

A preliminary characterisation of the noise of the stations was performed to inform later work. Figure 5 shows the spectral analysis of representative 1-hour periods of (velocity) data (at 11 am and 11 pm local time) on the 21st of May 2021 at the five stations. This date was chosen because all stations were known to be operating optimally at this time. The comparison of the three components shows a clear increase in noise during the night for the stations DHE and the noise and sensor recalibration complications affected station EDH. These two stations are in populated farms and roads so the higher noise during night could be due to traffic. The background noise for the 3 other stations remains largely the same. The night-time amplitude spectrum for the east component shows a slightly weaker peak at the HAY station compared to the rest of the stations which is visible at about 0.8 Hz for the east component.

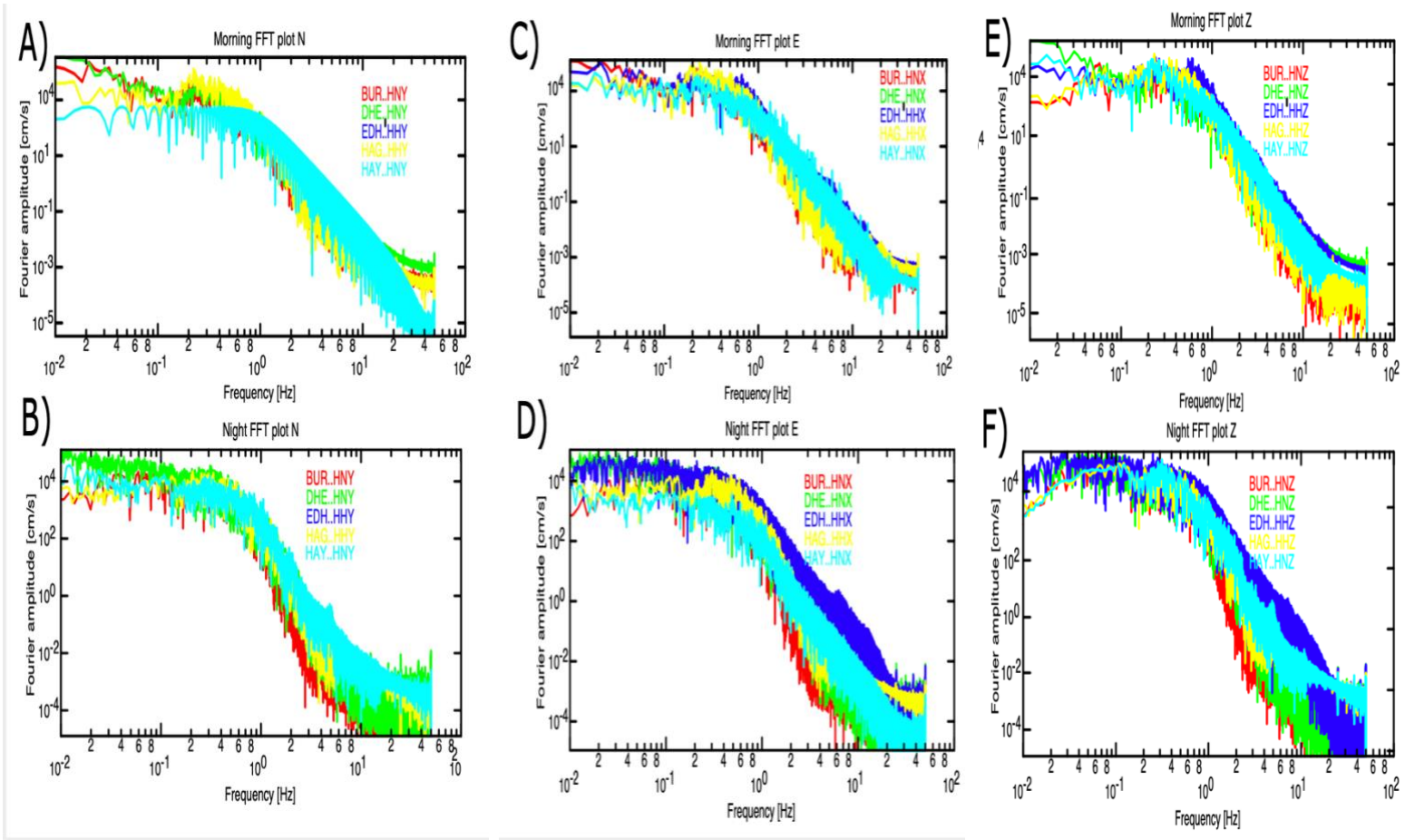

Figure 3.2. Comparison of the amplitude spectrum (between 0.01-100 seconds) for the three components at the 5 seismic stations for 60-minute recording intervals from 11 am for the morning plots and 11 pm for the night plots.

Chapter 4: Receiver Functions of Somaliland

4.1 Introduction

The receiver function is a time series analysis method of extracting constraints on the crust and upper mantle structure from teleseismic waveforms recorded at three component seismometers. The reverberations of primary body wave arrivals (generally the direct P- or S-phase) in near-surface structure appear in the coda of the main phase, and their amplitude and the arrival times can be modelled to constrain the underlying geology. The receiver function method has been widely used by seismologists in investigations of the crust and the upper mantle structure (e.g., Owens and Zandt 1985). The method's appeal stems from the underlying theory's relative simplicity, as well as its cost-effectiveness in harnessing teleseismic earthquakes as a source of energy. This method differs from others in that the wave energy approaches the seismometer from depth, sampling deep structures, which gives it advantages over controlled source methods (such as wide-angle reflection and refraction approaches).

In this chapter, we apply receiver function analysis to teleseismic earthquake data extracted from the seismic dataset described in Chapter 3, in order to constrain crustal thickness and seismic properties of the Somaliland margin of the Gulf of Aden rift.

4.2 The Receiver Function Method

The receiver function method is a time series technique which can be used to study crustal structures from observations of the travel times and amplitudes of the P to S wave conversion postcursory arrivals of the direct P-wave phase from teleseismic earthquakes (earthquakes with distances greater than 1000 km).

This time series technique was first used in 1977 (Burdick and Langston, 1977). They found using synthetic seismograms to model the S-wave arrivals in the P-wave coda that it is possible to accurately model the crust under seismic stations. They were able to identify a velocity discontinuity near a receiver by identifying energy in the SV component after the P-wave arrival as a P-S wave conversion from the base of the crust.

Such conversions arise from near-receiver interfaces encountered by the up-going primary wavefield; portions of the wavefield are refracted, converted to another wavetype and reflected (Figure 4.1). As a P-wave arrives from a teleseismic event when it reaches a seismic velocity discontinuity between two layers at an oblique angle it will polarize and split into a P-wave and (in isotropic media) an SV-wave. The P-wave travels faster than an S-wave, thus the P-wave will arrive first (Figure 4.1), and the Moho conversions and reflections will arrive in or after the P-wave coda. In addition to P-S conversions, the downgoing reflection at the free surface (crust-air interface) can cause further arrivals from multiples (e.g., PpPs, PsPs, PpPs) reflected back up from the Moho interface (figure 4.1).

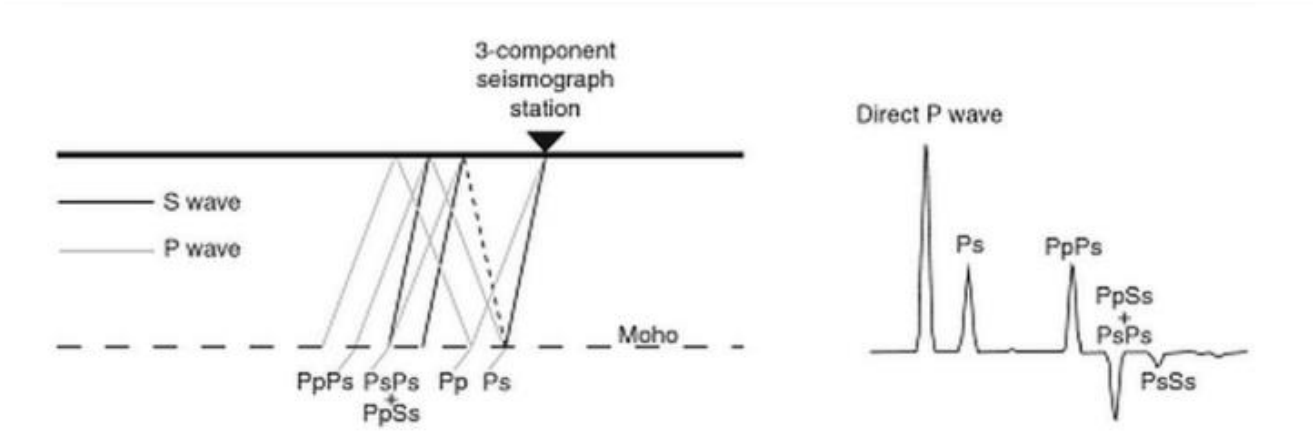

Figure 4.1. Illustration of raypaths for an incoming direct P wave (denoted Pp) and five of its conversions and reflections: Ps, PpPs PpPs etc. Note that while PpPs and PsPp have different raypaths, they arrive at the same travel time in the homogeneous two-layer case. Cartoon from Ammon (1991).

Both the amplitude and travel time of these arrivals contain considerable information about the thickness, seismic velocity and density of the crust.

The main difficulty in using these postcursors is their relatively low amplitude compared to the P-wave coda. The receiver function approach circumvents this by exploiting the different partitioning of energy for P and S phases between components of the seismogram, utilising the three-component nature of modern seismic stations (Figure 4.2).

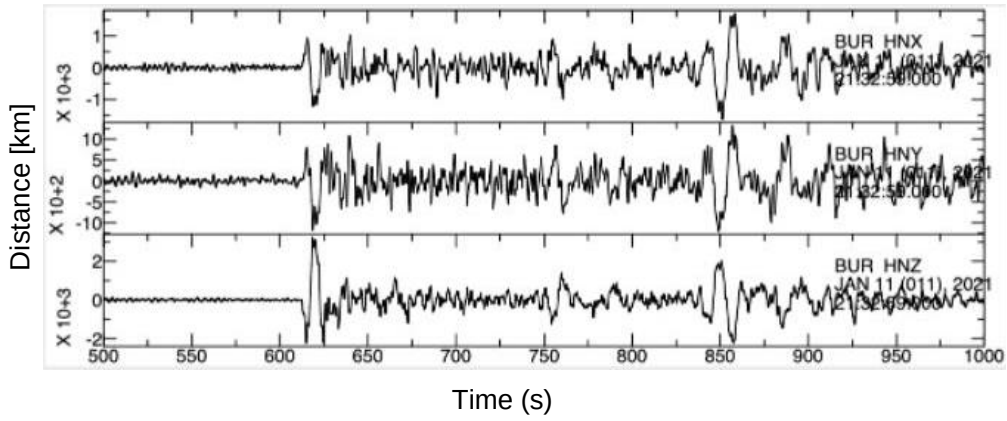

Figure 4.2. The East, North and vertical components of a seismogram recorded in BUR station during a teleseismic event.

4.2.1 Isolating and Enhancing the Converted Wavefield

If the horizontal components of the seismic data are rotated (by projection) from their (usual) North-East orientation to radial-transverse (where the radial direction denotes the backazimuth direction to the earthquake), for isotropic, homogeneous horizontal layers the P-wave primary and the S-wave conversions and reflections are isolated to the vertical and radial components. Energy appearing on the transverse component in this window is an indication that one or more of these conditions is violated (e.g., Stein and Wysession 2003). By itself the rotation to radial-transverse is normally insufficient to isolate the postcursory arrivals of interest. In order to enhance them, the vertical component is then deconvolved from the radial and transverse components, enhancing the crustal (and potentially mantle) reverberations directly beneath the receiver. This process enhances the signal in the low amplitude reverberations while simultaneously removing complications of the P-wave coda. The 'receiver function' thus generally refers to the resulting deconvolved radial and transverse components.

4.2.2 ETMTRF Deconvolution

Over the past century, receiver function methodologies have seen significant progress. Originally intended to operate in the frequency domain (Phinney, 1964) studies like Clayton and Wiggins (1976) extended it to work in the time domain. In this study we use the extended multi-taper frequency domain cross-correlation receiver function (ETMRF) estimation approach of Helffrich (2008). This is an adaptation of the Multi Taper Frequency-Domain Cross-Correlation Receiver Function (MTRF) developed by Park and Levin (2000) who

proposed a method which distinguishes between incoherent and coherent signals, he also distinguished that on both the vertical and horizontal components the inverse of the variance is weighted, which gives the coherent signal more weight in the frequency domain (Park and Levin. 2000). This method has several advantages, for example reducing the interference of microseism noise in the 0.1-0.5 Hz range giving an improved receiver function image (Helffrich, 2008).

The method is similar to the overlap-add method for evaluating the discrete convolution of in a long time series (Press et al., 1992). The difference with this technique lies with the preservation of the phase information. This technique retains phase information by creating a frequency domain representation that for each sub-window of the time series preserves the phase lags (Helffrich, 2008).

The approach initially follows a standard method for forming multi-taper spectral estimates whereby each taper windows the data for the whole analysis segment, and then the Fourier Transform is computed and added to any prior Fourier Transforms for that taper (Helffrich, 2008). After that the usual method for multi-taper spectral estimates form a receiver function estimate *HR(f)*. Park and Levin (2000) and Helffrich (2008) do this by estimating the noise at a specific frequency and using the pre-arrival Z-component as well as calculating the cross-correlation of the radial (R) component with the vertical (Z) component of the Fourier transform:

$$H_R(f) = \frac{\sum_{k=1}^{k} \left(Y_Z^{(k)}(f)\right) * Y_R^{(k)}(f)}{S_0(f) + \sum_{k=1}^{k} \left(Y_Z^{(k)}(f)\right) * Y_R^{(k)}(f)} \quad (4.1)$$

The R- or Z-component signals in this method are represented by the $Y_{R,Z}^{(k)}$ Slepian-tapered Fourier transforms (Helffrich, 2008), the pre-event noise on the vertical component is represented by $S_0(f)$, and the * operator denotes complex conjugation. A high-frequency cut-off is implemented in the receiver function by using a frequency domain taper of cos^2.This,

together with the various windows, results in the following normalising factors for the spectra (Helffrich, 2008):

$$\frac{1}{N_{window}} \times \frac{N_{ft}}{N_{fc}} \times \frac{2}{N_{ft}} \tag{4.2}$$

where N window is the number of windows that are contributing to the sum, N_{ft} is the number of points that are in the Fourier transform, and N_{fc} is the number of points in the cos^2taper that are non-zero. As a result, a receiver function with the same length as the original analysis segment is produced (Helffrich, 2008) (Figure 4.3).

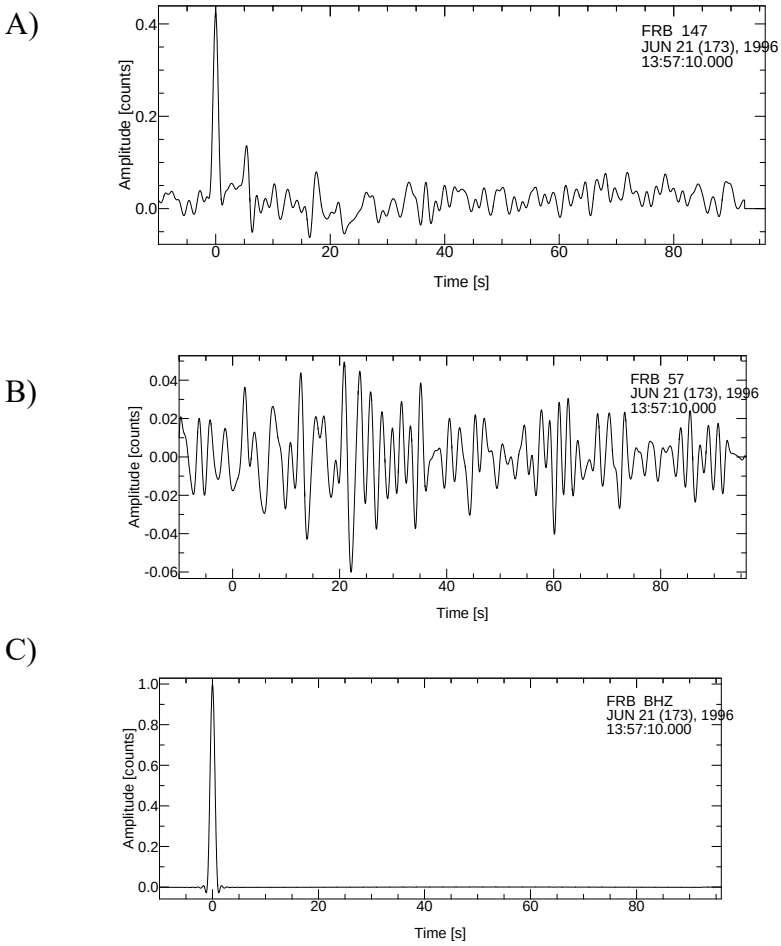

4.3 Somaliland Dataset

Figure 4.3. An example ETMTRF calculated receiver function of earthquake data from an event of the East coast of Kamchatka at station FRB in Nunavut, northern Canada showing Ps, PpPs and PpSs wave arrivals. Where: A- is the radial component, B- is the

4.3.1 Event Selection

We apply EMTRF to recordings of teleseismic events at the Somaliland seismic array (stations DHE, BUR, HAG) described in Chapter 3. We searched the IRIS global catalogue of earthquakes (through the WILBER3 service) to identify events meeting the following criteria:

- A minimum reported magnitude of 6 mb (to ensure favourable signal to noise ratio).
- An epicentral distance between 30° and 90°, within the distance range of teleseismic P.
- Occurring between 1st October 2020 – 31st July 2021 (covering the operational time of the Somaliland array).

This resulted in a list of 20 events, listed in Table 4.1, identified for further analysis. Figure 4.4 shows a map of the event locations.

	Month	Day	Time	Lat	Lon	Depth	Mag	Region
2020	11	7	01:10:32	25.71	143.60	16.0	5.8	Volcano Islands, Japan region
2020	11	15	22:37:43	8.76	126.29	43.0	6.0	5 km S of Marihatag, Philippines
2020	12	10	13:19:58	24.76	122.00	73.2	6.1	25 km E of Yilan, Taiwan
2020	12	14	19:35:58	72.24	0.76	10.0	5.8	Norwegian Sea
2020	12	15	23:21:57	5.18	125.42	14.0	6.1	25 km S of Sarangani, Philippines
2020	12	20	17:23:22	40.87	142.58	35.0	6.3	100 km ENE of Hachinohe, Japan
2020	12	23	18:11:47	6.25	133.63	11.0	6.1	90 km SW of Angaur State, Palau
2020	12	29	11:19:54	45.43	16.25	10.0	6.4	2 km WSW of Petrinja, Croatia
2021	1	23	23:36:50	-61.81	-55.49	9.8	6.9	South Shetland Islands
2021	2	7	04:22:57	6.75	125.17	24.9	6.0	2 km SW of Magsaysay, Philippines
2021	2	10	12:52:27	-5.68	101.65	10.0	6.2	218 km SSW of Bengkulu, Indonesia
2021	3	3	10:16:09	39.75	22.17	8.0	6.3	9 km W of T√Ωrnavos, Greece
2021	3	20	09:09:44	38.47	141.63	43.0	7.0	29 km ENE of Ishinomaki, Japan
2021	4	3	01:16:39	-58.01	-7.84	10.0	6.6	east of the South Sandwich Islands
2021	4	28	02:21:26	26.77	92.43	34.0	6.0	8 km NNW of Dhekiajuli, India
2021	5	1	01:27:27	38.22	141.66	47.3	6.8	38 km ESE of Ishinomaki, Japan
2021	5	12	14:05:15	-17.38	66.31	10.0	6.7	Mauritius - Reunion region
2021	5	14	06:33:07	0.13	96.64	11.0	6.7	260 km S of Sinabang, Indonesia
2021	5	21	18:04:13	34.58	98.24	10.0	7.3	Southern Qinghai, China
2021	5	21	13:48:37	25.74	100.01	9.0	6.1	26 km NW of Dali, China

Table 4.1. Details of all events identified for further study. Locations and magnitudes are from USGS Wilber3.

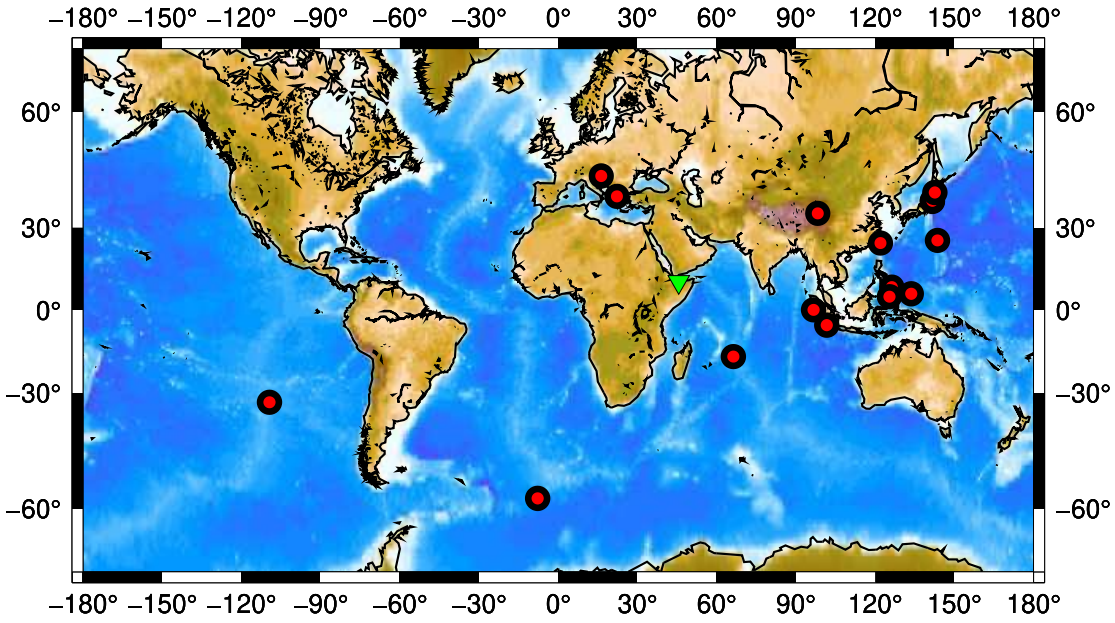

Figure 4.4. Epicentral locations (red circles) of events analysed in the receiver function study.

4.4 Receiver Function Analysis

The data for 60 minutes after each event at all stations were extracted from the SAC data archive, and event and station geometry were populated in the headers. The data were then cut to a hand-picked 100 second window around the P-wave arrival (following Helffrich, 2008), and band-pass filtered between corner frequencies of 0.01Hz to 1.0Hz (other, narrower filters were also tested but found to produce less useful data). At this point a visual inspection of all traces was performed to identify events and stations with a clear, unambiguous P-wave arrival (based on reference model travel times). This stage significantly reduced the available dataset. There were 12 useable events in total identified for three of the stations. No usable events were initially identified at EDH and HAY (even those with good signal at the other stations), due to high levels of noise (Chapter 3).

The data were rotated to the radial-transverse reference frame, and ETMRF deconvolution was applied to each event-station pair using a FORTRAN code (Helffrich, 2008). This resulted in 12 radial component receiver functions for three stations (Figures 4.5,4.6 and 4.7).

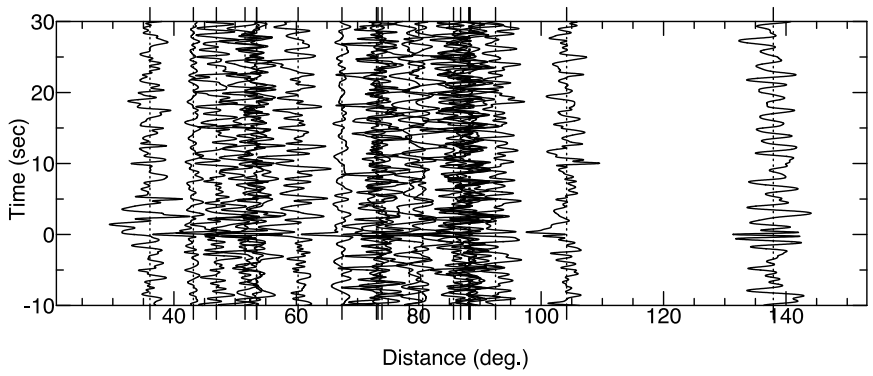

Figure 4.5. Radial receiver functions plotted against distance for the events recorded at HAG.

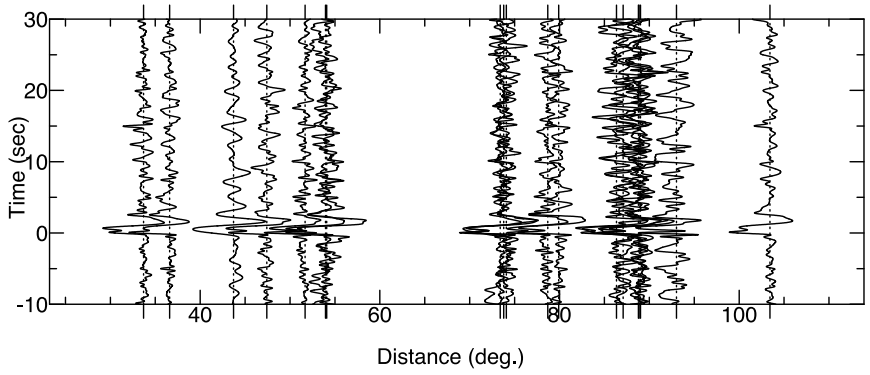

Figure 4.6. Radial receiver functions plotted against distance for the events recorded at BUR.

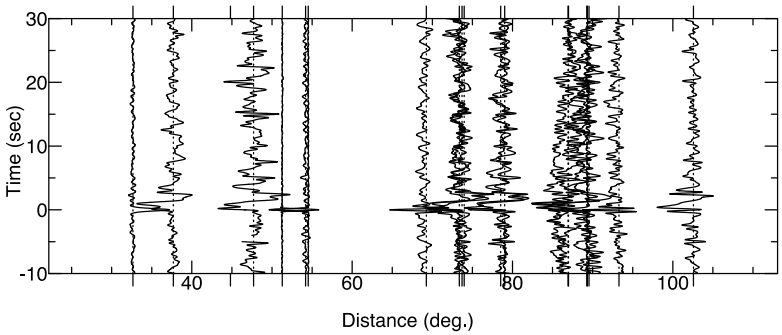

Figure 4.7. Radial receiver functions plotted against distance for the events recorded at DHE.

4.4.1 Receiver Function Stacking

The subsurface of the Earth is not uniform so all seismic occurrences encountered by the receiver has a unique structure. Thus, unique solutions will be produced from the receiver function deconvolution estimates. To show this uniqueness, the receiver functions for two events (South Shetlands and Philippines) recorded at BUR station are compared in Figure 4.8:

A)

B)

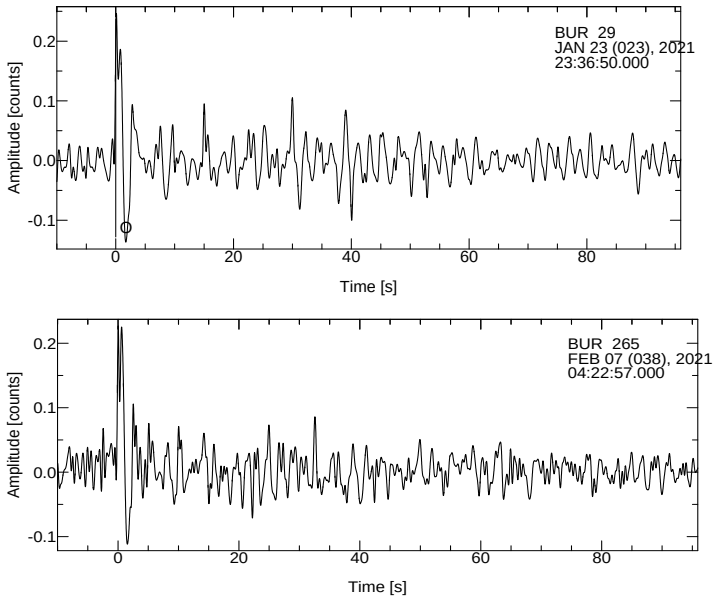

Figure 4.8. Receiver function comparisons from BUR station showing evidence converted phase arrivals. A is from an earthquake in South Shetlands and B is from an earthquake in Philippines.

The receiver functions have a few observable differences but appear to be mostly similar; this indicates that the receiver functions response was created by a similar subsurface. In more

complex subsurfaces the receiver function would generate more differing responses. Stacking individual receiver functions can reduce signal to noise ratio, and provide an average structural response. We perform linear stacking using the Signal Stacking Subprocess (SSS) in SAC over a time window of -10–30s, as this sufficiently includes the signal responses of interest (Figures 4.11-4.16).

4.4.2 H-κ Stacking

A priori information must be included since the usual receiver function study's range of slownesses is frequently insufficient to resolve the depth-velocity ambiguity (Ammon et al., 1990). Therefore, the H- κ stacking approach of Zhu and Kanamori (2000) was utilised to find final estimations of crustal structure and composition (Torsvik, 2015). The method employs a stacking algorithm to combine the directly incoming P-to-S conversion Ps with the later arriving multiple crustal reverberations (multiples) PpPs and PpPs + PpSs (Torsvik, 2015). The method's objective is to calculate the v_P/v_S ratio (κ) and crustal thickness (H) from the receiver function time series (e.g., Chevrot & Van der Hilst 2000).

A SAC programme called HK (Helffrich, pers. comm.) was used to carry out the H- κ calculation. The H- κ stacking technique's objective function is:

$$s(H,\kappa) = \sum_{j=1}^{N} w_1 r_j(t_1[H,\kappa]) + w_2 r_j(t_2[H,\kappa]) - w_3 r_j(t_3[H,\kappa]) \qquad (4.3)$$

The number of receiver functions used is *N*; the weights are: w_1, w_2 and w_3; and the receiver function amplitudes for receiver function number j at the anticipated arrival times of Ps (t_1), PpPs (t_2) and PpPs + PpSs (t_3) is $r_j\,(t)$. The following equations anticipate the three arrival times (Torsvik, 2015):

$$t_1 = H\left[\sqrt{\frac{1}{v_S^2} - p^2} - \sqrt{\frac{1}{v_P^2} - p^2}\right] \qquad (4.4)$$

$$t_2 = H\left[\sqrt{\frac{1}{v_S^2} - p^2} + \sqrt{\frac{1}{v_P^2} - p^2}\right] \quad (4.5)$$

$$t_3 = 2H\sqrt{\frac{1}{v_S^2} - p^2} \quad (4.6)$$

The horizontal slowness (s/° or s/km), also known as the ray parameter, is represented by the expression v_P, where v_P is an estimated average P-wave velocity through the crust assuming the crust is homogenous, and the Moho is flat and horizontal (Torsvik, 2015). The horizontal slowness was estimated for each event-station pair using the iasp91 reference model (Kennett and Engdahl, 1991).

The H-κ station procedure was applied to the set of receiver function traces for each station (HAG, BUR and DHE) to estimate crustal thickness and v_P/v_S ratio. v_P was assumed to be 6.5 km/s, and the objective function in equation (4.3) was evaluated for a grid search range between $20 \leq H \leq 50$ km, and $1.5 \leq \kappa \leq 2.0$, with increments at 0.05 km and 0.01 increments respectively.

4.4.3 Evaluation of Uncertainties

In order to estimate the uncertainties on the crustal thicknesses and the v_P/v_S ratio inferred from the H-κ stacking, a bootstrapping method was applied. Bootstrapping is a resampling method that enables non-linear problems error estimation (e.g., Menke, 2018), it can be advantageous for receiver function studies however it can be inaccurate for cases when the number of observations are limited (e.g., Park and Levin, 2016). The general principle of Parera-Portell's bootstrapping technique was applied to the H-κ stacking data (Parera-Portell et al., 2021). The method was applied by repeating the H-κ stacking with a randomly selected set of the receiver functions for each station for 1000 iterations. The distribution of the resulting population of crustal thickness and v_P/v_S ratios was analysed to determine the standard deviation – the errors arequoted as 2 standard deviations.

4.5 Results

The deconvolution of radial and vertical P wave seismograms yielded 20 suitable events (8 from the first tranche of data recovered and 12 from the second. These data were then used to estimate the crustal thicknesses beneath three stations (HAG, BUR and DHE). Stations EDH and HAY of the deployment were too noisy to produce clear arrivals on their corresponding receiver functions and were not sufficiently high quality to yield unambiguous results.

The data from the 3 stations was further tested by dividing their receiver functions into groups depending on their backazimuths the H-κ results were then revaluated to see if they yielded any different results. This, however, did not affect the results signficantsly.

Results of the H-κ grid search and bootstrapping analysis for HAG, BUR and DHE are reported in Table 4.2 and Figures 4.11 to 4.16. These results are presented as crustal thickness and v_P/v_S surfaces. The parameters derived from the complete dataset are within one standard deviation of *H* and *k* derived from the bootstrapping, and because of this, we report the latter values as our final crustal thickness. The crustal thicknesses obtained for HAG was $33 \pm 2.50\ km$ with a v_P/v_S ratio of 1.95 ± 0.15, BUR had a crustal thickness of $38 \pm 4.00\ km$ with a v_P/v_S ratio of : 1.80 ± 0.20 and DHE had a crustal thickness of $34 \pm 2.50\ km$ with a v_P/v_S ratio of 1.66 ± 0.10 (Table 4.2).

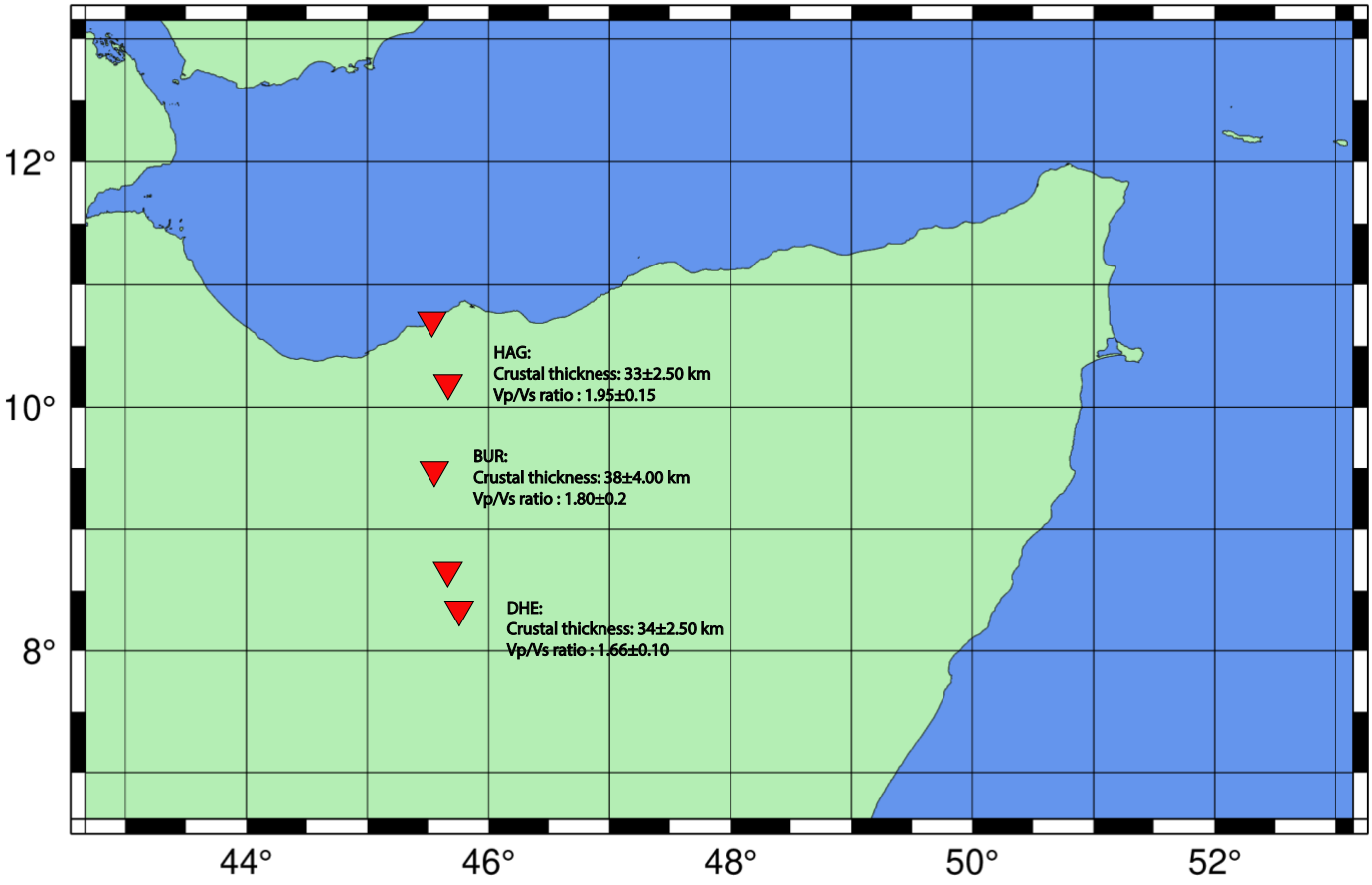

Figure 4.9. Map of Somaliland with the crustal thicknesses and vP/vS ratios at the stations for which we have a robust result.

4.6 Interpretation and Discussion

4.6.1 Crustal Thickness

The crustal thickness measured at the stations suggest a general trend of increasing from north to south are identified with the crust is at its thickest in the mountainous regions near BUR station where the crustal thickness reaches a maximum of 38±4 km. We note, however, that strictly the crustal thickness is just about within error of each other, so we cannot completely rule out a constant thickness.

To test this trend further, we revisit EDH, a station which did not produced a coherent result in our first pass analysis. By grouping the receiver functions by backazimuth, and producing H-κ stacks for each group, we were able to get a reasonable result using only the receiver functions from events in Philippines and China Table 4.1. The resulting stack produces a crustal model with a crustal thickness of ~23 km and a v_P/v_S ratio of ~1.60 (the scarcity of stations invalidates the calculation of the errors using the bootstrapping). While we do not consider this result as robust as the others, it is consistent with considerably thinned crustal compared to the stations to the south.

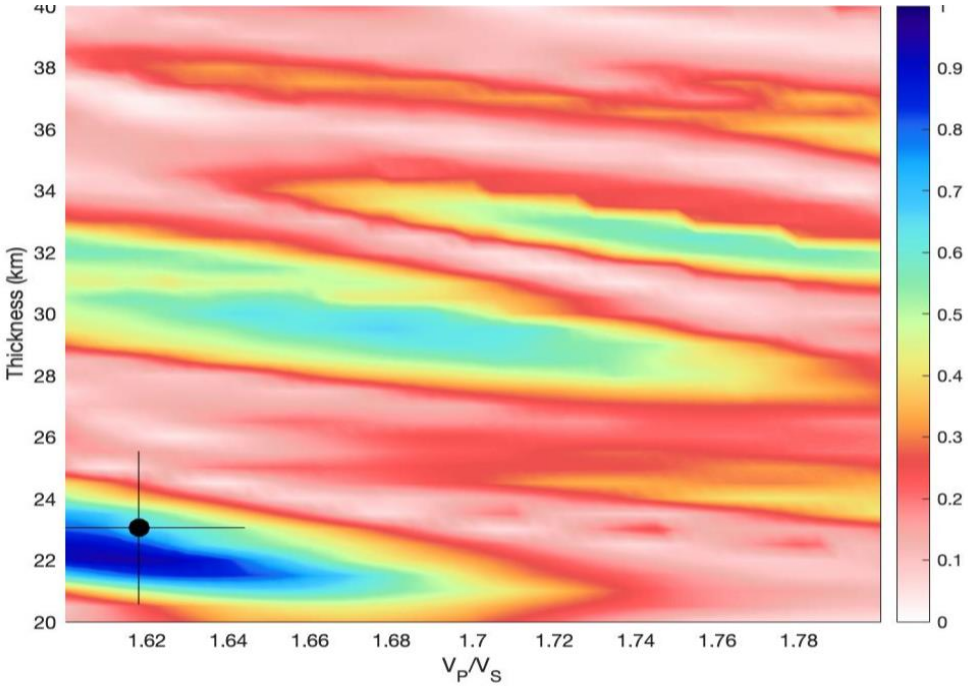

Figure 4.10. Backazimuth H– κ stacking plot for EDH station. In the stacked H–K result, the best fit is indicated by the black cross. The colour bar shows the stacked amplitude at the predicted times for reverberation at the corresponding crustal thickness vp/vs ratio.

4.6.2 v_P/v_S

From the receiver function to the north HAG the station yields k-values of ~1.95 $\pm$0.15, the BUR station yields a k-value of ~1.80 $\pm$0.20 (Figure 4.11-4.16). To the south the DHE station's k-value is relatively low, averaging ~1.66 $\pm$0.10. It is evident that the k-values are inconsistent across the 3 stations HAG appears to have a higher v_P/v_S ratio than the other 2 stations. The v_P/v_S ratio for the HAG station was restricted from a range of 1.6-2.1 to a range of 1.6-1.8 due to no viable results detected in the given range for the v_P/v_S ratio. The results obtained for the v_P/v_S ratios are similar to the global average which is ~1.74 for the crust (Zhu, 2018).

4.6.3 Comparison with Backstripping

We interpret crustal thickness differences between HAG and BUR as resulting from the rifting the region has undergone throughout its history (Ali and Watts, 2013). Ahmed et al., (2014) interprets the pre rifting crustal thickness to be 35 km based on seismic refraction data and receiver function analysis in Yemen, which is within error of our results.

Our results reflect the great effect inflicted by the rifting events described in Chapter 2. The studies of the backstripping curves (Chapter 2) can give an insight as to how the crustal structure and thinning was formed and what rifting sequences effected the crust. From the backstripping data its evident that the area has undergone periods of rifting, this is reflected by our seismic results where there is a disparity in the crustal thicknesses across the 4 seismic stations. The backstripping curves also show characteristic features of the accelerated subsidence (figure 2.2) a concave up profile with a quick initial subsidence and a gradual later subsidence (Ali and Watts, 2013), this could be due to the crust and lithosphere heating up and being thinned during rifting. which can explain the trend of a decrease in crustal thicknesses from north to south seen from BUR to HAG (Ali and Watts, 2013).

The v_P/v_S ratio across the three seismometers are not uniform, there is an observed transition from ~1.95 to ~1.80 to ~1.66 (from north to south). This range is difficult to reconcile with the observed geology as there is no suggestion of decrease in mafic rocks further south. Experiments in the lab have demonstrated that κ values, as they relate to Poisson's ratio, are

influenced by the quantity of silica in the crust (Tarkov and Vavakin, 1982). The higher the amounts of silica, the lower the obtained k values, resulting in more mafic crust typically yielding typically higher k values, on the order of ~1.85, in contrast to felsic crust which yields values of ~1.7 (Tarkov and Vavakin, 1982). This is not obviously consistent with HAG station's observed v_P/v_S of ~1.95 as HAG is located near ultramafic basement rocks. However, the observed κ values had a high error, the κ value for DHE: 1.95 ± 0.15 was within the error of BUR: 1.80 ± 0.2 and the K value of BUR was within the error of HAG: 1.66 ± 0.1.

4.6.4 Comparison with Yemen Data

There have been a few geophysical studies in Somaliland (Ali and Watts, 2013; Ali and Watts, 2015), but none directly analysing crustal thickness. However, Yemen is also a reasonable source of comparison. Somaliland and Yemen share a rifting history – the Somaliland (north-western Somalia)-Yemen conjugate margin which formed after the opening of the Gulf of Aden and after the rifting of the African and Arabian plates (Ali and Watts, 2013), it might be expected that (in a broad sense) the crustal structure of Somaliland might mirror that of western Yemen (on the opposite side of the Gulf of Aden). Moreover, Socotra Island, located between the Guardafui Channel and the Arabian Sea (Figure 1.2), while significantly east, lies a similar distance to (and on the same side of) the ridge axis and so may also yield an interesting comparison.

Ahmed et al., (2013) estimates of crustal thickness vary from 23 km in the coastal areas to 35–36 km below the Yemen plateau. This trend effectively mirrors our results which suggest a crustal thickness of 23 km from at the station closest to the coast (EDH) and 38 km south at BUR. The average v_P/v_S ratio in western Yemen is comparable to that of Somaliland; it is 1.79 for the western Yemen Plateau and increases to 1.92 towards the Red Sea coast, which is comparable to our average of 1.8 ± 0.20 increasing to 1.95 ± 0.15 north towards the Gulf of Aden.

The Island of Socotra (Figure 1.2) has also been quite extensively studied with receiver functions. Across the western region of Socotra, Ahmed et al., (2014) suggests crustal thickness increasing from north to south from ~ 16.5 km in the northern region to ~ 35-40

km. This trend of increasing thickness southwards is interpreted as being due to the three Oligocene rifting sequences which are also observed in our findings from backstripping. Ahmed et al., (2014) observes that the receiver functions in western Socotra don't image the Conrad discontinuity (unlike Western Yemen) and attributes it to the crust having been strongly affected by the Oligo-Miocene rifting. This is supported by interpretations from an ENCENs cruise (Leroy et al., 2010) across the northeastern Gulf of Aden which demonstrates that there is no velocity step when the velocity increases gradually from 6.0 km/s (upper crustal velocity) to 7.0 km/s (lower crustal velocity) in the continental domain, this could mean that the upper crust is being removed or that the composition of the crust has changed in conjunction with the substantial thinning of the crust (Ahmed et al., 2014). Similarly, there is no evidence of the Conrad discontinuity in the Somaliland region which should be sighted between a depth of 7.5 and 14 km (Ahmed et al., 2014).

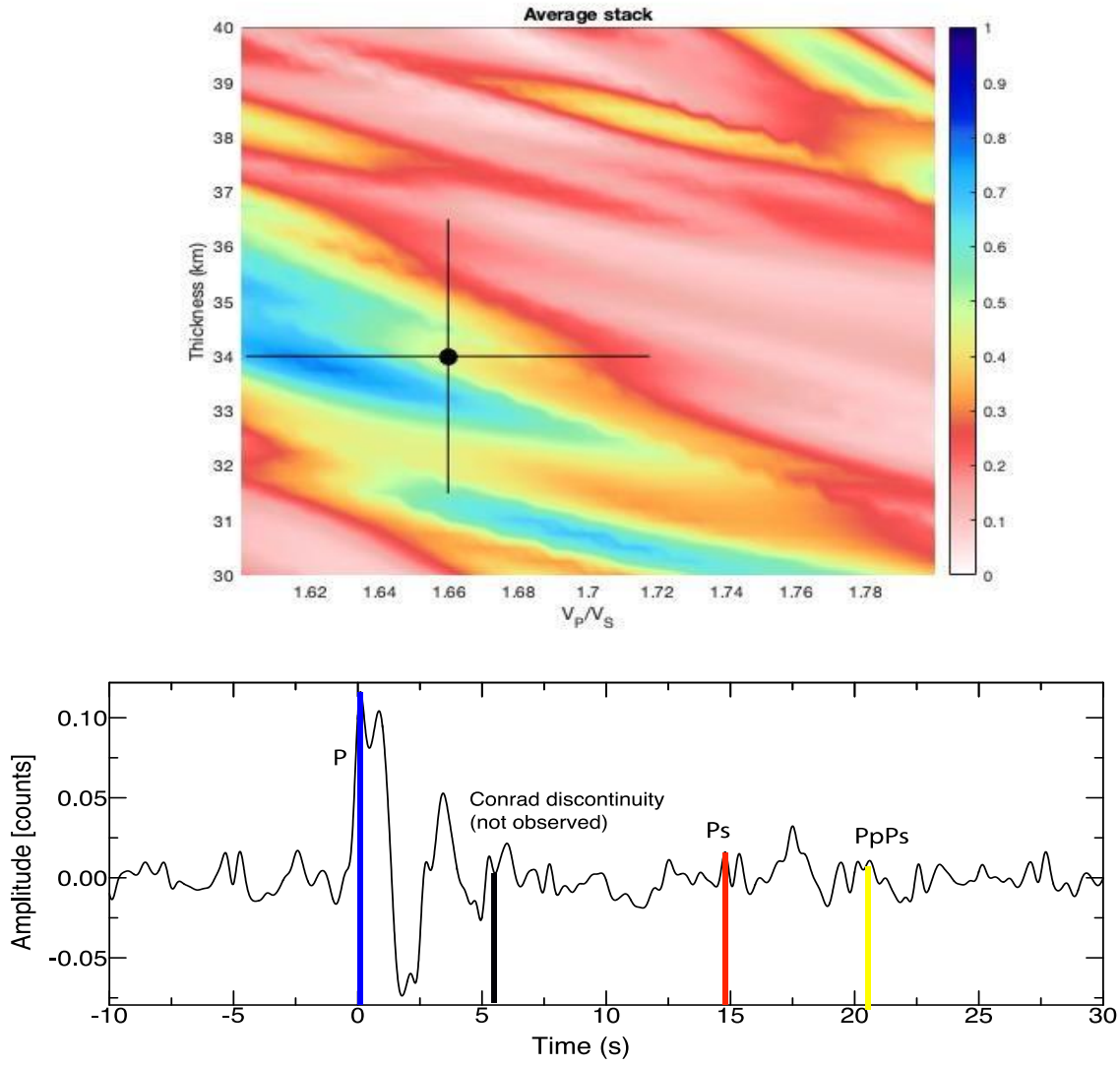

Fig 4.11 and 4.12 (DHE).

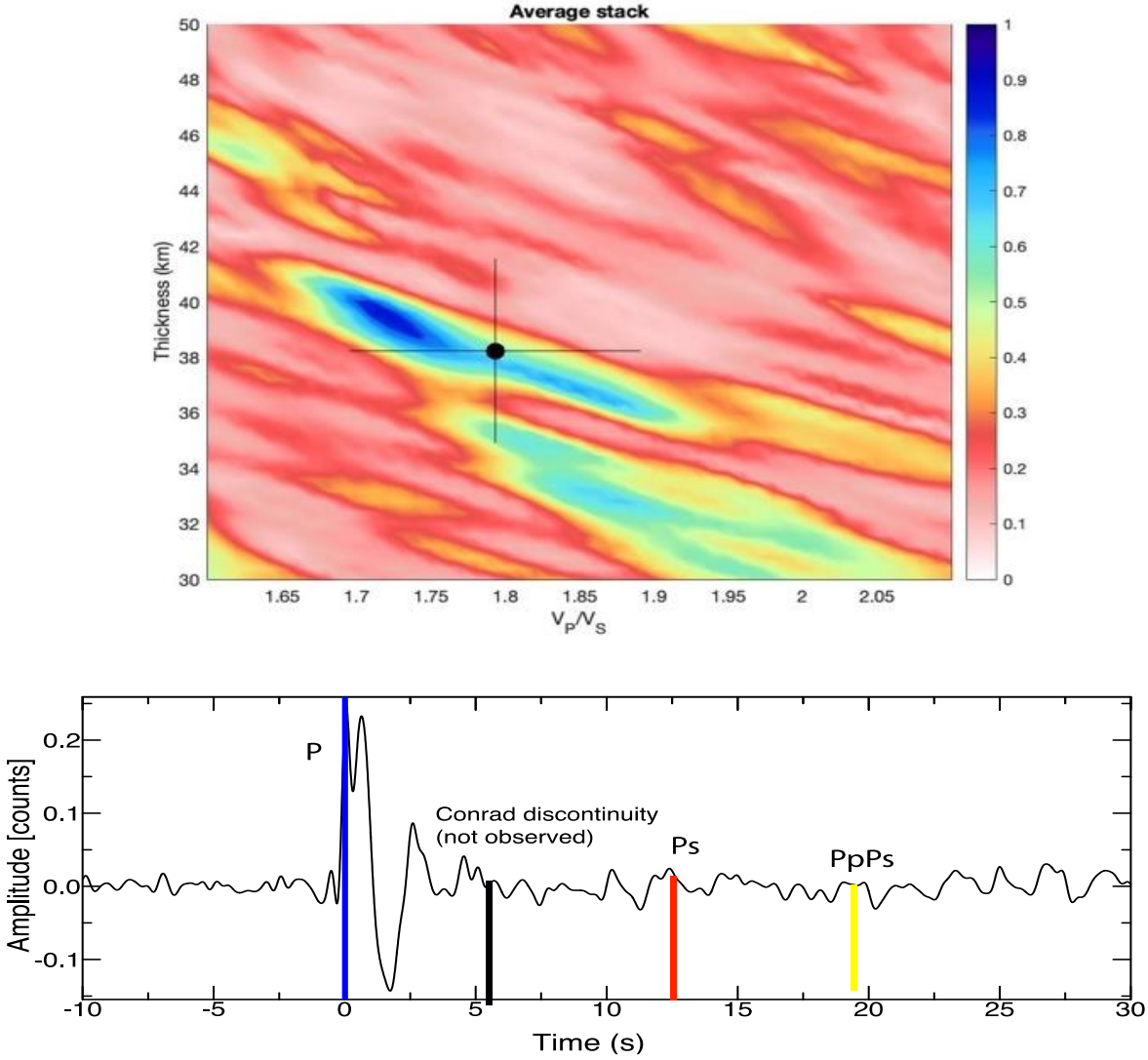

Fig 4.13 and 4.14 (BUR).

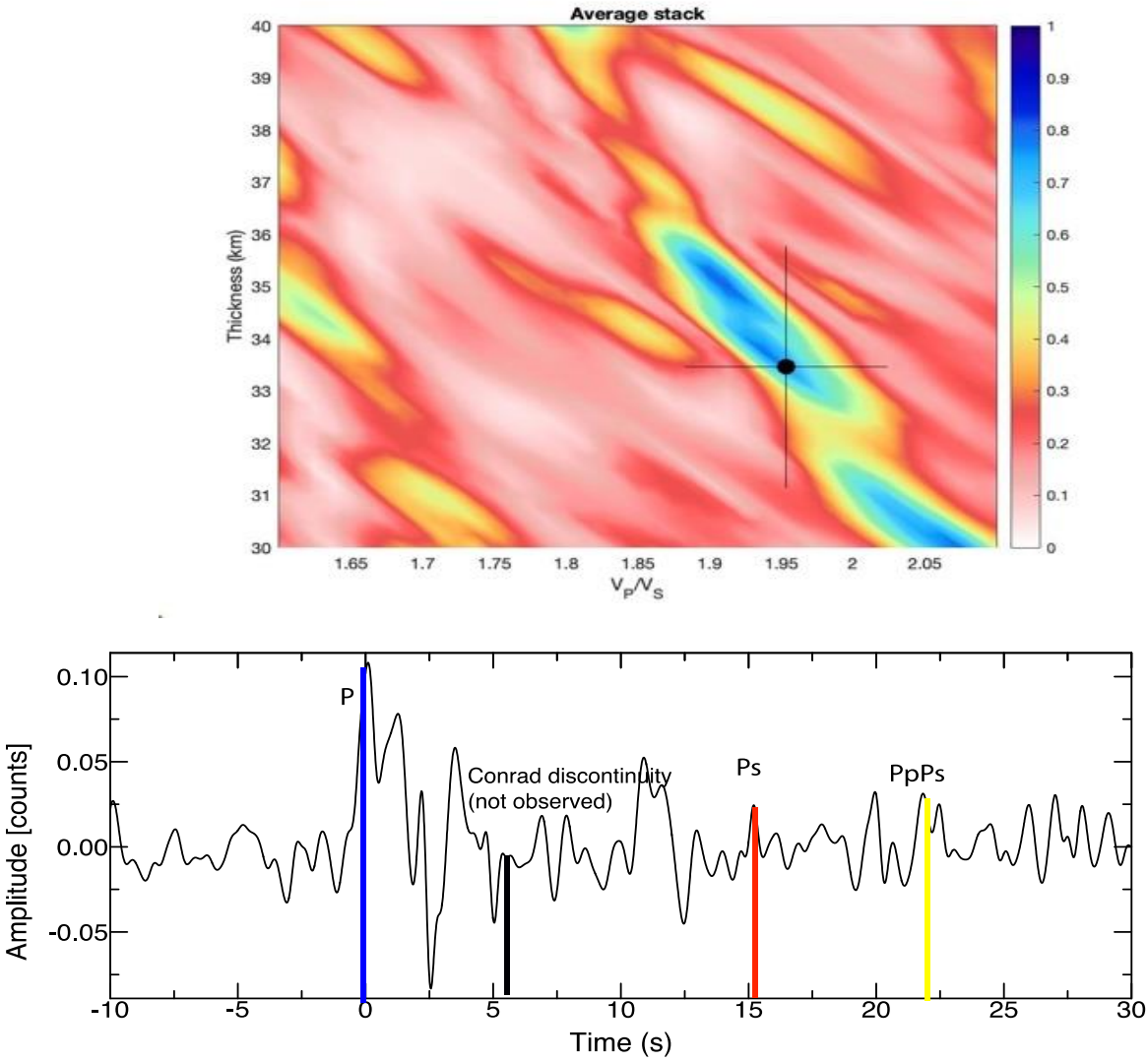

Fig 4.15 and 4.16 (HAG).

Figure 4.11-4.16. H–K stacking for DHE, BUR and HAG. In the stacked H–K result, the best fit is indicated by the black cross. Rf's showing wave arrivals with each figure focused on the best solution. The colour bar shows the stacked amplitude at the predicted times for reverberation at the corresponding crustal thickness vp/vs ratio. The picks are observed from the H–K model.

Station Name	Number of Viable RF	Latitude (N)	Longitude (E)	Elevation (M)	Crustal thickness (km)	v_P/v_S ratio	Error in depth (km)	Error in v_P/v_S
EDH	[2]	10.75869°	45.60419°	13	[23]	[1.60]	[±2.50]	[±0.02]
HAG	13	10.25256°	45.74044°	380	33	1.95	±2.50	±0.15
BUR	12	09.51717°	45.56362°	1010	38	1.80	±4.00	±0.20
HAY	-	8.71734°	45.73534°	799	-	-	-	-
DHE	12	8.39776°	45.83372°	763	34	1.66	±2.50	±0.10

Table 4.2. Receiver function and H-κ bootstrap results for the Somaliland seismometers.

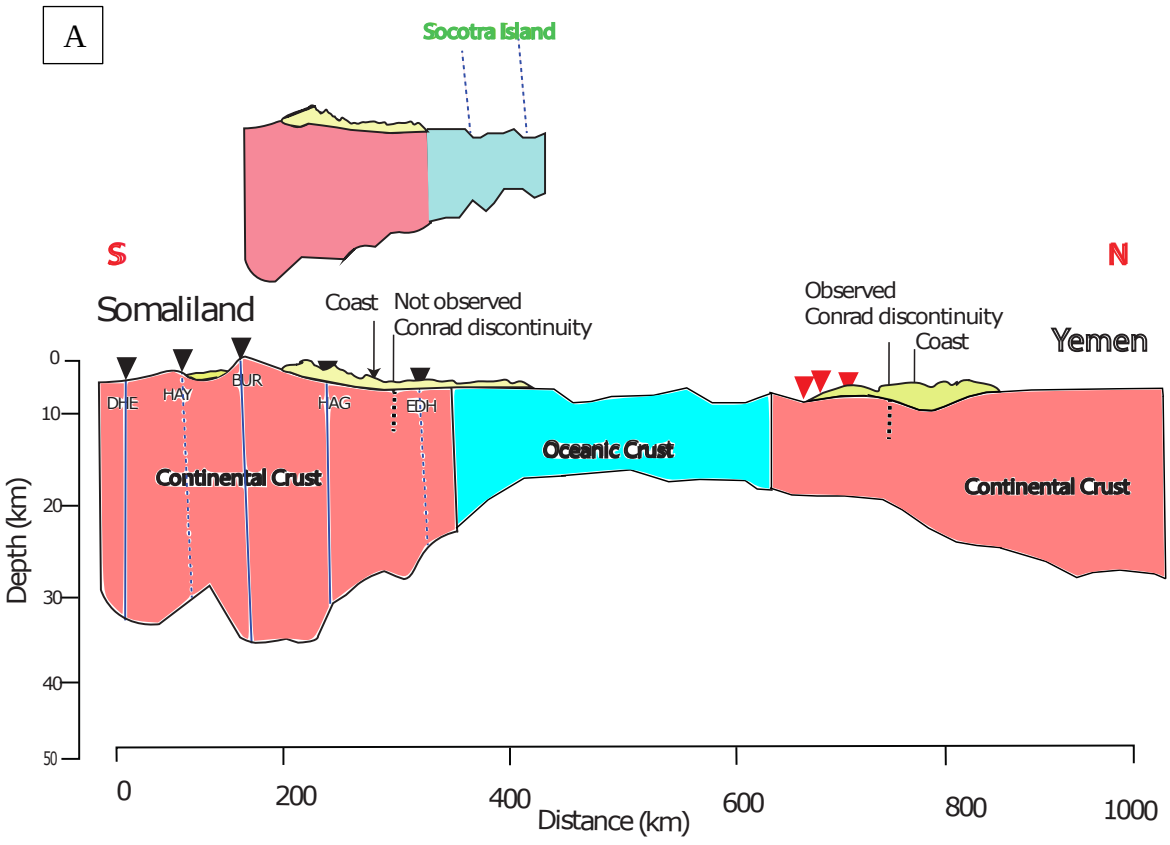

B

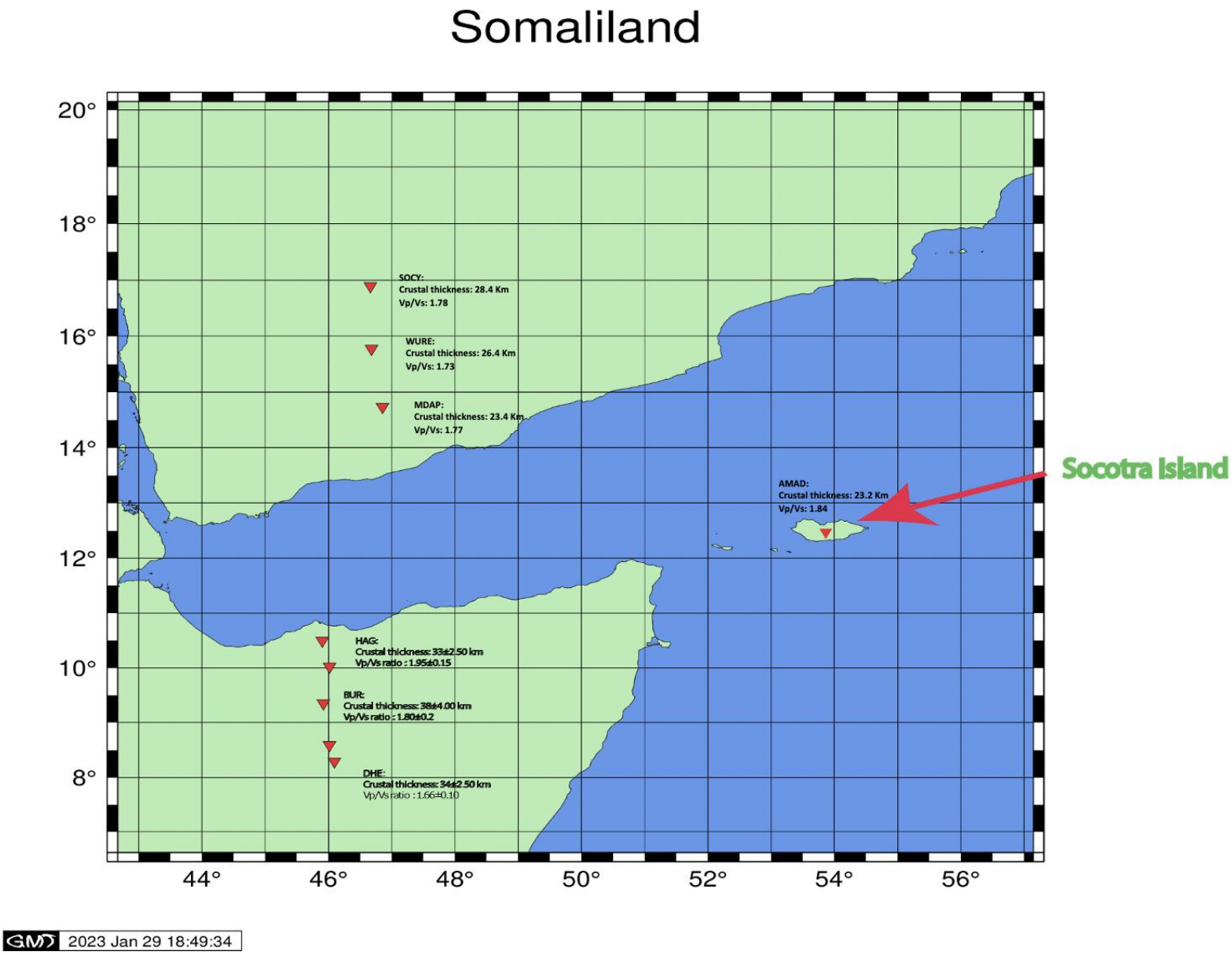

Figure 4.12 Figure A displays a cross section of Somaliland and Yemen with the approximate thicknesses also displayed showcasing the approximate thicknesses as reported by Ahmed et al. (2014). Figure B is a map displaying the approximate locations of some of the seismometers used in this study.

Chapter 5: Conclusions

5.1 Overview of the Thesis

Somaliland is located in the northern part of Somalia, with the Gulf of Aden to the North and Ethiopia to the west. Somaliland is located near intersections of three major plate boundaries the Red Sea and Gulf of Aden oceanic spreading ridges, as well as the continental East African Rift system. Somaliland's morphology resembles areas that have undergone extension such as Yemen, not a lot of folding is seen in the region however there is a significant amount of normal faulting (Ali, 2015).

Information about crustal development can be obtained using detailed study of stratigraphic information, from for example, borehole data. In this thesis we have repeated the backstripping study of Ali and Watts (2015) with a modified porosity model in order to provide insight into the crustal development of Somaliland. Our results are virtually identical to those of the earlier study, showing the method is not sensitive to the fine detail of the porosity model assumed. The backstripping curves suggest four main tectonic features, which we associate with rifting events over the past 160 Myr. The first of which is a Kimmeridgian-Tithonian (145 Ma-157 Ma) rift phase its characterised by accelerating subsidence from ~157 Ma to ~148 Ma. Another tectonic feature that was observed is uplift in early to late cretaceous (100 Ma- 145 Ma) it was characterised by shallower subsidence curves suggesting a decrease in subsidence possibly due to due to post rift thermal subsidence. A second rift phase is observed during Campanian-Maastrichtian epoch (84 Ma- 66Ma) characterised by a period (~80 Ma to ~48 Ma) of rapid subsidence. The third rift sequence is observed during Oligocene-Miocene epoch (23 Ma- 33Ma) it is characterised by faster rate of subsidence from 32 Ma- ~28 Ma.

Such approaches, however, do not provide a direct constraint on crustal structure. Unlike in Yemen, on the other side of the Gulf of Aden, there are no previous geophysical studies directly imaging (for example) crustal depth in Somaliland.

To provide these direct constraints, in this project we have deployed a small network of five broadband stations across Somaliland (Figure 4.17) to investigate the crustal structure of Somaliland.

Using 9 months of data from this network, we have generated seismic receiver functions for 20 events at the 5 stations in the network (Table 4.1). Of these, 3 stations produced robust results with approximately 12 viable receiver functions per station. We have applied the H-κ stacking method of Zhu and Kanamori (2000) to measure crustal thickness and v_P/v_S ratio, using a bootstrapping approach to estimate constraint. This analysis shows that the crust beneath Somaliland apparently increases in thickness from North to South, away from the coast (from 33 ±3km to 38 ±4km). v_P/v_S ratios appear to be inconsistent across the three stations with the HAG the station yielding k-values of ~1.95 $\pm$0.15, the BUR station yielding k-values of ~1.80 $\pm$0.20 and the DHE station yielding relatively low k-values averaging ~1.66 $\pm$0.10 (Table 4.2). The northernmost station EDH experienced significant noise interference and was not used for the primary analysis however when the receiver functions were restricted into backazimuths groups the resulting model suggests a crustal thickness of ~23 km and a v_P/v_S ratio of ~1.60 its consistent with the trend of increasing crustal thickness from the northern to the southern region of Somaliland (Figure 4.10).

We attribute this change in crustal thickness to the intensive rifting processes experienced by the region (e.g., Ali and Watts, 2013; 2015). We have also compared our estimates of crustal properties with those measured for Yemen (Ahmed et al 2014), which lies on the other side of the Gulf of Aden rift. These data show that a trend of increasing crustal thickness northwards across western Yemen, mirroring the structure we have measured. The average v_P/v_S ratio in western Yemen is also comparable to that of Somaliland; it is 1.79 for the western Yemen Plateau and increases to 1.92 towards the Red Sea coast, which is comparable to our average of 1.8 increasing to 1.95 north towards the Gulf of Aden. Unlike in Western Yemen, we see no evidence for a Conrad discontinuity, suggesting strong tectonic activity. Finally, we show that the structure we have measured has parallels on Socotra Island to the east, further along the rift.

5.2 Future Work

There are still unknown factors about the crustal structure of Somaliland, which further work could be done to address. The seismometer array used in this survey needs to be expanded from three to at least twenty with a more along the coast and deployed longer to get more teleseismic earthquakes, and thus better estimates for the crustal thicknesses and a more representative crustal image of Somaliland as well as to improve signal to noise ratio on RFs. There are possibilities for more advanced analysis (such as RF migration) to study more complex structure. Other seismic techniques such as joint inversion with gravity data can be used alongside receiver functions to enhance the accuracy of our result as joint inversion helps reduce the uncertainties (e.g., Guo et al., 2019). If a larger array was deployed, and allowed to collect data for long enough, a range of other techniques would be possible. Surface wave studies and/or ambient noise interferometry could be applied to study crustal velocity structure (e.g, Ma and Clayton, 2016). Such a deployment could also allow the study of the shallow mantle beneath the rift, for example using travel-time tomography (e.g., Vinnik et al., 2004), seismic anisotropy (e.g., Licciardi et al., 2016) and discontinuity studies.

References

Ahmed, A., Leroy, S., Keir, D., Korostelev, F., Khanbari, K., Rolandone, F., Stuart, G. and Obrebski, M. (2014). Crustal structure of the Gulf of Aden southern margin: Evidence from receiver functions on Socotra Island (Yemen). *Tectonophysics*, 637, pp.251–267. doi:10.1016/j.tecto.2014.10.014.

Ahmed, A., Tiberi, C., Leroy, S., Stuart, G.W., Keir, D., Sholan, J., Khanbari, K., Al-Ganad, I. and Basuyau, C. (2013). Crustal structure of the rifted volcanic margins and uplifted plateau of Western Yemen from receiver function analysis. *Geophysical Journal International*, 193(3), pp.1673–1690. doi:10.1093/gji/ggt072.

Ali, M.Y. (2009). Geology and coal potential of Somaliland. *International Journal of Oil, Gas and Coal Technology*, 2(2), p.168. doi:10.1504/ijogct.2009.024885.

Ali, M.Y. (2015). Petroleum Geology and Hydrocarbon Potential of the Guban Basin, Northern Somaliland. *Journal of Petroleum Geology*, 38(4), pp.433–457. doi:10.1111/jpg.12620.

Ali, M.Y. and Watts, A.B. (2013). Subsidence history, crustal structure, and evolution of the Somaliland-Yemen conjugate margin. *Journal of Geophysical Research: Solid Earth*, 118(4), pp.1638–1649. doi:10.1002/jgrb.50113.

Ali, M.Y. and Watts, A.B. (2015). Tectonic evolution of sedimentary basins of northern Somalia. *Basin Research*, 28(3), pp.340–364. doi:10.1111/bre.12113.

Allen, P.A. and Allen, J.R. (2005). *Basin analysis: principles and applications*. Malden, MA USA: Blackwell Pub.

Allen, P.A. and John Richard Allen (2013). *Basin analysis: principles and application to petroleum play assessment*. Chichester, West Sussex, UK: Wiley-Blackwell.

Ammon, C.J. (1991). The isolation of receiver effects from teleseismic P waveforms. *Bulletin of the Seismological Society of America*, 81(6), pp.2504–2510. doi:10.1785/bssa0810062504.

Ammon, C.J., Randall, G.E. and Zandt, G. (1990). On the nonuniqueness of receiver function

inversions. *Journal of Geophysical Research*, 95(B10), p.15303. doi:10.1029/jb095ib10p15303.

Angevine, C.L., Heller, P.L. and Paola, C. (1990). *Quantitative sedimentary basin modeling*. Tulsa, OK, USA: American Association Of Petroleum Geologists.

B, W.A. and S, S.M. (1979). Subsidence and eustasy at the continental margin of eastern North America. [online] American Geophysical Union (AGU), pp.218–234. doi:https://doi.org/10.1029/ME003p0218.

Bastow, I.D., Stuart, G.W., Kendall, J-Michael. and Ebinger, C.J. (2005). Upper-mantle seismic structure in a region of incipient continental breakup: northern Ethiopian rift. *Geophysical Journal International*, 162(2), pp.479–493. doi:10.1111/j.1365-246x.2005.02666.x.

Bosellini, A. (1986). East Africa continental margins. *Geology*, 14(1), p.76. doi:10.1130/0091-7613(1986)14<76:eacm>2.0.co;2.

Bosellini, A. (1992). The continental margins of Somalia: Structural evolution and sequence stratigraphy. [online] American Association of Petroleum Geologists. doi:10.1306/M53552C11.

Bossuyt, F. and Milinkovitch, M.C. (2001). Amphibians as Indicators of Early Tertiary 'Out-

of-India' Dispersal of Vertebrates. *Science*, 292(5514), pp.93–95. doi:10.1126/science.1058875.

Bosworth, W., et al. (2020). The role of tectonic activity in shaping the future evolution of the Red Sea and Gulf of Aden. Geological Society, London, Special Publications, 506(1), 1-28. https://doi.org/10.1144/SP506-2020-115

Bosworth, W., Stockli, D., and Saltzer, R. (2020). "Tectonic evolution of the Red Sea and Gulf of Aden: introduction and overview," Geological Society, London, Special Publications, 540, 1-22.

Buck, R. (2004). 1. Consequences of Asthenospheric Variability on Continental Rifting. pp.1–30. doi:10.7312/karn12738002.

Burdick, L.J. and Langston, C.A. (1977). Modeling crustal structure through the use of converted phases in teleseismic body-wave forms. *Bulletin of the Seismological Society of America*, 67(3), pp.677–691. doi:10.1785/bssa0670030677.

Cande, S.C. and Stegman, D.R. (2011). Indian and African plate motions driven by the push force of the Réunion plume head. *Nature*, 475(7354), pp.47–52. doi:10.1038/nature10174.

Chevrot, S. and van der Hilst, R.D. (2000). The Poisson ratio of the Australian crust: geological and geophysical implications. *Earth and Planetary Science Letters*, 183(1-2), pp.121–132. doi:10.1016/s0012-821x(00)00264-8.

Clayton, R.W. and Wiggins, R.A. (1976). Source shape estimation and deconvolution of teleseismic bodywaves. *Geophysical Journal International*, 47(1), pp.151–177. doi:10.1111/j.1365-246x.1976.tb01267.x.

Cloetingh, S., Burov, E., Matenco, L., Beekman, F., Roure, F. and Ziegler, P.A. (2013). The Moho in extensional tectonic settings: Insights from thermo-mechanical models. *Tectonophysics*, 609, pp.558–604. doi:10.1016/j.tecto.2013.06.010.

Cochran, J.R. (1981). The Gulf of Aden: Structure and evolution of a young ocean basin and continental margin. *Journal of Geophysical Research*, [online] 86(B1), p.263. doi:10.1029/jb086ib01p00263.

Cochran, J.R., Goff, J.A., Malinverno, A., Fornari, D.J., Keeley, C. and Wang, X. (1993)

Morphology of a ‘superfast’ Mid-Ocean Ridge crest and flanks: The East Pacific Rise. Earth and Planetary Science Letters, 119(1-2), pp.85-104.

Coffin, M.F. and Rabinowitz, P.D. (1987). Reconstruction of Madagascar and Africa: Evidence from the Davie Fracture Zone and Western Somali Basin. *Journal of Geophysical Research*, 92(B9), p.9385. doi:10.1029/jb092ib09p09385.

Doglioni, C. (2008). Plate Tectonics. pp.117–134.

Dugda, M.T. (2005). Crustal structure in Ethiopia and Kenya from receiver function analysis: Implications for rift development in eastern Africa. *Journal of Geophysical Research*, 110(B1). doi:10.1029/2004jb003065.

Ellis, A.C., Kerr, H.M., Cornwell, C.P. and Williams, D.O. (1996). A tectono-stratigraphic framework for Yemen and its implications for hydrocarbon potential. *Petroleum Geoscience*, 2(1), pp.29–42. doi:10.1144/petgeo.2.1.29.

Fairhead, J.D. and Girdler, R.W. (1972). The seismicity of the East African rift system. *Tectonophysics*, 15(1-2), pp.115–122. doi:10.1016/0040-1951(72)90056-x.

Fang, P., Ding, W., Zhao, Y., Lin, X. and Zhao, Z. (2022). Detachment-controlled subsidence pattern at hyper-extended passive margin: Insights from backstripping modelling of the Baiyun Rift, northern South China Sea. *Gondwana Research*. doi:10.1016/j.gr.2021.12.012.

Hughes, G.W and Beydoun, Z.R. (1992). The Red Sea—Gulf of Aden: biostratigraphy, lithostratigraphy and palaeoenvironments. *Journal of Petroleum Geology*, 15. doi:10.1306/bf9ab701-0eb6-11d7-8643000102c1865d.

G., A. W., & MacFadyen, W. A. (1933). The Geology of British Somaliland. Part I of the Geology and Palaeontology of British Somaliland. The Geographical Journal, 82(6), 545-572. doi:10.2307/1785483.

Geolsoc.org.uk. (2012). *The Geological Society*. [online] Available at: https://www.geolsoc.org.uk/Plate-Tectonics/Chap3-Plate-Margins/Divergent/Triple-Junction.

Guo, L., Gao, R., Shi, L., Huang, Z. and Ma, Y. (2019). Crustal thickness and Poisson’s ratios of South China revealed from joint inversion of receiver function and gravity data. *Earth and Planetary Science Letters*, 510, pp.142–152. doi:10.1016/j.epsl.2018.12.039.

Haberland, C. and Ritter, O. (2016). GIPP: Geophysical Instrument Pool Potsdam. *Journal of large-scale research facilities JLSRF*, 2. doi:10.17815/jlsrf-2-128.

Hamoudi, M., Kusznir, N.J., Gaina, C., and Doubrovine, P.V. (2019). "Evolution of the Gulf of Aden: Insights from magnetic anomaly inversion and plate kinematic modeling," Journal of Geophysical Research: Solid Earth, 124(6), 6346-6373.

Helffrich, G. (2008). Erratum to Extended-Time Multitaper Frequency Domain Cross-Correlation Receiver-Function Estimation. *Bulletin of the Seismological Society of America*, 98(3), pp.1608–1608. doi:10.1785/0120080022.

Holt, P. (2012) *Subsidence Mechanisms of Sedimentary Basins Developed over Accretionary Crust*, Durham theses, Durham University. Available at Durham E-Theses Online: http://etheses.dur.ac.uk/3584/

Honda, H. (1962). Earthquake Mechanism and Seismic Waves. *Journal of Physics of the Earth*, 10(2), pp.1–97. doi:10.4294/jpe1952.10.2_1.

Hunt, J.A. (1942). Geology of the Zeila Plain, British Somaliland. *Geological Magazine*, 79(3), pp.197–201. doi:10.1017/s0016756800073738.

Jiaren, Y. and Mingde, L. (1997). Geohistory Modelling of Cratonic Basins: A Case Study of the Ordos Basin, NW China. *Journal of Petroleum Geology*, 20(3), pp.347–362. doi:10.1111/j.1747-5457.1997.tb00640.x.

Johnson, W.J. and Clark, J.C. (1992). Improving Subsurface Resolution with the Seismic Reflection Method: Use S-waves. *Ground Water Management*, 11(655-663).

Kendall, J.-M. and Lithgow-Bertelloni, C. (2016). Why is Africa rifting? *Geological Society, London, Special Publications*, 420(1), pp.11–30. doi:10.1144/sp420.17.

Kennett, B.L.N. and Engdahl, E.R. (1991). Traveltimes for global earthquake location and phase identification. *Geophysical Journal International*, 105(2), pp.429–465. doi:10.1111/j.1365-246x.1991.tb06724.x.

Kusznir, N.J., Almalki, K.A., and Gaina, C. (2018). "Tectonic controls on the development of the Red Sea and Gulf of Aden rift systems: An overview," Geological Society, London,

Special Publications, 469(1), 1-33.

Leroy, S., Lucazeau, F., d'Acremont, E., Watremez, L., Autin, J., Rouzo, S., Bellahsen, N., Tiberi, C., Ebinger, C., Beslier, M.-O., Perrot, J., Razin, P., Rolandone, F., Sloan, H., Stuart, G., Al Lazki, A., Al-Toubi, K., Bache, F., Bonneville, A. and Goutorbe, B. (2010). Contrasted styles of rifting in the eastern Gulf of Aden: A combined wide-angle, multichannel seismic, and heat flow survey. Geochemistry, Geophysics, Geosystems, 11(7), n/a-n/a. doi: 10.1029/2009GC002963.

Leroy, S., Razin, P., Autin, J., Bache, F., d'Acremont, E., Watremez, L., Robinet, J., Baurion, C., Denele, Y., Bellahsen, N., Lucazeau, F., Rolandone, F., Rouzo, S., Kiel, J., Robin, C., Guillocheau, F., Tiberi, C., Basuyau, C., Beslier, M. and Allazki, A. (2012). From rifting to oceanic spreading in the Gulf of Aden: A synthesis. *Arabian Journal of Geosciences*, 5. doi:10.1007/s1251701104754.

Leroy, S., Bellahsen, N., Hamimi, Z., Münch, P., and Autin, J. (2019). "Geodynamic evolution of the Red Sea and Gulf of Aden: introduction and overview," Geological Society, London, Special Publications, 468(1), 1-21.

Leroy, S., Autin, J., d'Acremont, E., Mouchot, N., Ahmed, A. S., Roest, W. R., & Dorbath, C. (2019). Multiple phases of rifting and volcanism along the Red Sea and Gulf of Aden margins. Geology, 47(6), 503-507. doi: 10.1130/G46072.1

Levin, V., Park, J., Brandon, M.T. and Menke, W. (2000). Thinning of the upper mantle during late Paleozoic Appalachian orogenesis. *Geology*, 28(3), p.239. doi:10.1130/0091-7613(2000)28<239:totumd>2.0.co;2.

Licciardi, A. and Piana Agostinetti, N. (2016). A semi-automated method for the detection of seismic anisotropy at depth via receiver function analysis. *Geophysical Journal International*, 205(3), pp.1589–1612. doi:10.1093/gji/ggw091.

Lovering, J.F. (1958). The nature of the Mohorovicic discontinuity. *Transactions, American Geophysical Union*, 39(5), p.947. doi:10.1029/tr039i005p00947.

Ma, Y. and Clayton, R.W. (2016). Structure of the Los Angeles Basin from ambient noise and receiver functions. *Geophysical Journal International*, 206(3), pp.1645–1651. doi:10.1093/gji/ggw236.

Macfadyen, W.A. (1933). *The geology of British Somaliland*. London: Crown Agents for the Colonies.

Martín-Martín, M. and Robles-Marín, P. (2020). Alternative methods for calculating compaction in sedimentary basins. *Marine and Petroleum Geology*, 113, p.104132. doi:10.1016/j.marpetgeo.2019.104132.

Mason, J.E. (1957). An Isolated Occurrence of Igneous Rocks at Gorei in the Las Anod District of the Somaliland Protectorate. *Geological Magazine*, 94(6), pp.498–502. doi:10.1017/s0016756800070199.

Mckenzie, D. (1978). Some remarks on the development of sedimentary basins. *Earth and Planetary Science Letters*, [online] 40(1), pp.25–32. doi:10.1016/0012-821x(78)90071-7.

Menke, W. (2018). *Geophysical data analysis: discrete inverse theory*. Fourth edition. ed. [online] London, United Kingdom: Elsevier Ltd. Available at: http://www.vlebooks.com/vleweb/product/openreader?id=none&isbn=9780128135563.

Miller, K.G. (2005). The Phanerozoic Record of Global Sea-Level Change. *Science*, [online] 310(5752), pp.1293–1298. doi:10.1126/science.1116412.

Muller, R.D., Sdrolias, M., Gaina, C., Steinberger, B. and Heine, C. (2008). Long-Term Sea-Level Fluctuations Driven by Ocean Basin Dynamics. *Science*, [online] 319(5868), pp.1357–1362. doi:10.1126/science.1151540.

Nichols, G. and Watchorn, F. (1998). Climatic and geomorphic controls on rift sedimentation: Oligo-Miocene syn-rift facies in the Gulf of Aden, Yemen. *Marine and Petroleum Geology*, 15(6), pp.505–518. doi:10.1016/s0264-8172(98)80001-9.

Owens, T.J. and Zandt, G. (1985). The response of the continental crust-Mantle boundary observed on broadband teleseismic receiver functions. *Geophysical Research Letters*, 12(10), pp.705–708. doi:10.1029/gl012i010p00705.

Owens, T.J., Zandt, G. and Taylor, S.R. (1984). Seismic evidence for an ancient rift beneath the Cumberland Plateau, Tennessee: A detailed analysis of broadband teleseismicPwaveforms. *Journal of Geophysical Research: Solid Earth*, 89(B9), pp.7783–7795. doi:10.1029/jb089ib09p07783.

Parera-Portell, J.A., Mancilla, F. de L., Morales, J., Almendros, J. and Jiménez-Morales, V. (2021). Structure of the crust and upper mantle beneath the Bransfield Strait (Antarctica) using P receiver functions. *Tectonophysics*, 802, p.228744. doi:10.1016/j.tecto.2021.228744.

Park, J. and Levin, V. (2016). Statistics and frequency-domain moveout for multiple-taper receiver functions. *Geophysical Journal International*, 207(1), pp.512–527. doi:10.1093/gji/ggw291.

Phinney, R.A. (1964). Structure of the Earth's crust from spectral behavior of long-period body waves. *Journal of Geophysical Research*, 69(14), pp.2997–3017. doi:10.1029/jz069i014p02997.

Ringler, A.T. and Hutt, C.R. (2010). Self-Noise Models of Seismic Instruments. *Seismological Research Letters*, 81(6), pp.972–983. doi:10.1785/gssrl.81.6.972.

Roberts, A.M., Kusznir, N.J., Yielding, G. and Styles, P. (1998). 2D flexural backstripping of extensional basins; the need for a sideways glance. *Petroleum Geoscience*, 4(4), pp.327–338. doi:10.1144/petgeo.4.4.327.

Roger, B.W. (2004). Rheology and Deformation of the Lithosphere at Continental Margins. In: G.D. Karner, B. Taylor, N.W. Driscoll and D.L. Kohlstedt, eds. [online] Columbia University Press, pp.1–30. doi:doi:10.7312/karn12738002.

Sapin, F., Ringenbach, J.-C. . and Clerc, C. (2021). Rifted margins classification and forcing parameters. *Scientific Reports*, 11(1). doi:10.1038/s41598-021-87648-3.

Sleep, N.H. (2006). Mantle plumes from top to bottom. *Earth-Science Reviews*, 77(4), pp.231–271. doi:10.1016/j.earscirev.2006.03.007.

Steckler, M.S., Mountain, G.S., Miller, K.G. and Christie-Blick, N. (1999). Reconstruction of Tertiary progradation and clinoform development on the New Jersey passive margin by 2-D backstripping. *Marine Geology*, 154(1-4), pp.399–420. doi:10.1016/s0025-3227(98)00126-1.

Steckler, M.S. and Watts, A.B. (1978). Subsidence of the Atlantic-type continental margin off New York. *Earth and Planetary Science Letters*, 41(1), pp.1–13. doi:10.1016/0012-821x(78)90036-5.

Su, P., He, H., Tan, X., Liu, Y., Shi, F. and Kirby, E. (2021). Initiation and Evolution of the

Shanxi Rift System in North China: Evidence From Low-Temperature Thermochronology in a Plate Reconstruction Framework. *Tectonics*, 40(3). doi:10.1029/2020tc006298.

Swarbrick, R. (2012). Review of pore-pressure prediction challenges in high-temperature areas. *The Leading Edge*, 31(11), pp.1288–1294. doi:10.1190/tle31111288.1.

Taylor, S.K., Nicol, A. and Walsh, J.J. (2008). Displacement loss on growth faults due to sediment compaction. *Journal of Structural Geology*, 30(3), pp.394–405. doi:10.1016/j.jsg.2007.11.006.

Tiberi, C., Leroy, S., d'Acremont, E., Bellahsen, N., Ebinger, C., Al-Lazki, A. and Pointu, A. (2007). Crustal geometry of the northeastern Gulf of Aden passive margin: localization of the deformation inferred from receiver function analysis. *Geophysical Journal International*, 168(3), pp.1247–1260. doi:10.1111/j.1365-246x.2006.03294.x.

Torsvik, A 2015 'Receiver function analysis Seismic imaging of the crust beneath TROLL seismic station in Queen Maud Land, Antarctica', Master Thesis, University of Oslo, Oslo

van der Land, C., Wood, R., Wu, K., van Dijke, M.I.J., Jiang, Z., Corbett, P.W.M. and Couples, G. (2013). Modelling the permeability evolution of carbonate rocks. *Marine and Petroleum Geology*, 48, pp.1–7. doi:10.1016/j.marpetgeo.2013.07.006.

Vinnik, L.P., Reigber, C., Aleshin, I.M., Kosarev, G.L., Kaban, M.K., Oreshin, S.I. and Roecker, S.W. (2004). Receiver function tomography of the central Tien Shan. *Earth and Planetary Science Letters*, 225(1-2), pp.131–146. doi:10.1016/j.epsl.2004.05.039.

Watremez, L., Leroy, S., Rouzo, S., d'Acremont, E., Unternehr, P., Ebinger, C., Lucazeau, F. and Al-Lazki, A. (2011). The crustal structure of the north-eastern Gulf of Aden continental margin: insights from wide-angle seismic data. *Geophysical Journal International*, [online] 184, pp.575–594. doi:10.1111/j.1365-246X.2010.04881.x.

Watts, A.B. and Ryan, W.B.F. (1976). Flexure of the lithosphere and continental margin basins. *Tectonophysics*, 36(1-3), pp.25–44. doi:10.1016/0040-1951(76)90004-4.

Zhu, H. (2018). High Vp/Vs ratio in the crust and uppermost mantle beneath volcanoes in the Central and Eastern Anatolia. *Geophysical Journal International*, 214(3), pp.2151–2163. doi:10.1093/gji/ggy253.

Zhu, L. and Kanamori, H. (2000). Moho depth variation in southern California from teleseismic receiver functions. *Journal of Geophysical Research: Solid Earth*, 105(B2), pp.2969–2980. doi:10.1029/1999jb900322.